Comparison of temperature and wind between ground-based remote sensing observations and NWP model profiles in complex topography: the Meiringen campaign

Alexandre Bugnard[1], Martine Collaud Coen[1], Maxime Hervo[1], Daniel Leuenberger[1], Marco Arpagaus[1], and Samuel Monhart[1]

[1]Federal Office of Meteorology and Climatology, MeteoSwiss, Switzerland

Correspondence: Martine Collaud Coen (martine.collaud@meteoswiss.ch)

Abstract. Thermally driven valley winds and near-surface air temperature inversions are common over complex topography and have a significant impact on the local and mesoscale weather situation. They both affect the dynamics of air masses and pollutant concentration. Valley winds affect them by favoring horizontal transport and exchange between the boundary layer and the free troposphere, whereas temperature inversion concentrates pollutants in cold stable surface layers. The complex interactions that lead to the observed weather patterns are challenging for Numerical Weather Prediction (NWP) models. To study the performance of the COSMO-1E model analysis (KENDA-1), a measurement campaign took place from October 2021 to August 2022 in the 1.5 km wide Swiss Alpine valley called Haslital. A Microwave Radiometer and a Doppler Wind Lidar were installed at Meiringen, in addition to a multitude of automatic ground measurement stations recording meteorologic surface variables. Near the measurement sites, a low altitude pass, the Brünig Pass, influences the wind dynamic similarly to a tributary. The collected data shows frequent nighttime temperature inversions for all months under study, which persist during daytime in colder months. An extended thermal wind system was also observed during the campaign, except in December and January, allowing an extended analysis of along and cross valley winds. The comparison between the observations and the KENDA-1 data provides good model performances for monthly temperature and wind medians but frequent and important differences for single profiles, especially in case of particular events such as foehn. Modeled nighttime ground temperature overestimations are common due to missed temperature inversions resulting in a bias up to 8 °C. Concerning the valley wind system, modeled flows are similar to the observations in their extent and strength, but suffer from a too early morning transition time towards up valley winds. The findings of the present study allow to better understand the temperature distributions, the thermally driven wind system in a medium size valley, the interactions with tributary valley flows, as well as the performances and limitations of a model in such complex topography.

Keywords. Complex topography, Remote sensing, NWP, Temperature inversion, Valley winds, Foehn

1 Introduction

Over mountainous areas, interactions between the terrain and the overlying atmosphere favor the horizontal and vertical transports of moisture and pollutants. The complex topography of the Alps consequently increases the air masses exchanges

along the valleys and between the boundary layer and the free troposphere (De Wekker and Kossmann, 2015; Rotach et al., 2022). Both theoretical studies and experimental campaigns demonstrated that complex topography creates circulations with small and large space and time pattern (Lehner and Rotach, 2018). In valleys, the superposition of the various processes leads to a complex vertical layering in the mountainous boundary layer, which strongly depends on the specific conditions of the surrounding terrain in each studied valley. For Numerical Weather Prediction (NWP) models, simulation of the atmosphere over complex terrain requires not only dense and accurate horizontal and vertical grids to parameterize the mountainous terrain (Sekula et al., 2019) but also good estimates of vegetation, soil characteristics, net radiation, and speed of the large-scale flow (Adler et al., 2021). Difficulties of models directly related to complex topography comprise among others the representation of ground-based temperature (T) inversions, of thermal valley winds and particularly of foehn events.

During calm clear nights, the air T in valleys can fall below the T measured across the surrounding hill tops leading to cold-air pooling and associated T inversions in mountainous regions (Miró et al., 2018; Joly and Richard, 2019). T inversions influence fog formation (Chachere and Pu, 2017), vertical dilution of pollutants (Duine et al., 2017; Diémoz et al., 2019) and the development of the boundary layer during daytime (Schnitzhofer et al., 2009). Such inversion are favored in complex topography (Joly and Richard, 2018) and persists longer in deeper valleys, whereas inversion lifetimes converge to the one over a plain for wide valleys (Colette et al., 2003).

However, the small-scale nature of these near surface stable layers means that they are often poorly represented even in the highest resolution operational NWP models (Vosper et al., 2013). The quality predictions for near surface variables during stable conditions depends on locally generated circulations that are controlled by many factors such as turbulence, shortwave and longwave radiation, advection and subsidence. Deficiencies in the parametrization of the fluxes, especially during stable conditions, are well known (Hauge, 2006) and thus a finer grid resolution is needed in increasingly steep terrain (Sfyri et al., 2018). Simulations also underline the high sensitivity to the choice of the vertical grid in the prediction of cold pool formation and suggest that the vertical resolution near the surface is more important than the height of the lowest level (Vosper et al., 2013). However, the assimilation of measurements, not only of surface data but also of profiling observations (Crezee et al., 2022), may improve the NWP performance for surface T inversions (Martinet et al., 2017).

Thermally driven winds primarily occur under fair-weather conditions (Zardi and Whiteman, 2013). They develop due to differential heating of adjacent air masses. They can partially be explained by the topographic amplification factor concept (Whiteman, 1990) and local subsidence in the valley center induced by up-slope flow (Schmidli and Rotunno, 2010) leading to a faster heating of the air masses in the valley than over the plain. The valley–plain T contrast then produces an along-valley pressure gradient that induces strong up-valley wind during the day and more shallow down-valley wind during the night. Slope winds are air mass movements parallel to the slope induced by buoyancy force in the presence of air layers at different T. Slope winds move upward during the day and downward at night and play an important role in the morning and evening transition of along valley winds. However, slope winds evolve over shorter time scales than valley winds (Serafin et al., 2018).

The transition periods of up and down along valley winds are mostly driven by the sunrise and sunset. Even though minor changes in the topography can lead to a significant change in the flow regimes (Lang et al., 2015), some common features are observed among the existing studies. In general, the morning transition happens with a certain delay with respect to sunrise

caused by the time required for up slope winds and warm subsidence to erode the nocturnal T inversion. However, wind intensity can be heavily related to tributary valleys (Zängl, 2004) and therefore highly depends on the local topography. In the evening, as soon as the surface radiative balance becomes negative, the cold air formed at the surface moves down the slope and converges in the valley floor, which reverses the flow direction from up-valley to down-valley winds.

Synoptic winds coupled with wind channeling effects can however superpose on the above described thermal mountain winds (Jacques-Coper et al., 2015). This large scale flows present no defined diurnal cycle and are generally stronger than the thermal valley winds. Their effect on the valley wind system is highly variable and depends on the orientation of the synoptic flow with respect to the valley axis (Kossmann and Sturman, 2003; Rotach et al., 2015).

The capability of mesoscale NWP models to calculate the above described diurnal valley winds in real valleys has been investigated in a few studies (Chow et al., 2006; Langhans et al., 2013; Giovannini et al., 2017; Schmidli et al., 2018; Schmid et al., 2020; Adler et al., 2021; Schmidli and Quimbayo-Duarte, 2023). Globally, a good agreement between modeled and observed valley winds is achieved provided that spatial resolution of the models and surface data (e.g. snow cover and soil moisture) are high enough (Rotach et al., 2015). The size of the valley has an impact on the accuracy of the modeled winds (Schmidli et al., 2018). Generally, a closer agreement between the model and measurements was found for the smaller spatial resolution, which allows a better representation of the topography. (Wagner et al., 2014) shows that the grid resolution should be about 10 to 20 times smaller than the relevant topographic scale to fully capture the different exchange processes. Hence, increased grid resolution generally improves the performance of numerical simulations, which is even more pronounced if surface and soil model fields are accurately initialized (Langhans et al., 2013; Schmidli and Quimbayo-Duarte, 2023).

Finally, the performance of models to handle foehn events had been shown to be poor, with a cold bias over the whole profile bottom part (<1000 m) of valleys (Jansing et al., 2022; Tian et al., 2022; Saigger and Gohm, 2022) and wind speeds generally higher, both above crest height and within the valley.

Although the surface measurement network is relatively well distributed over the Alps, T and wind profile measurements by remote sensing (REM) instruments are rarely operationally performed in the Alpine valleys. However, a precise knowledge of the T structure of the atmosphere in complex terrain is essential for NWP models and the use of REM observations is a solution to obtain sufficient space/time resolution of the fast varying meteorological conditions in valleys.

The campaign in the Haslital provides a unique set of observations including a long period of observation (ten months comprising winter and summer months), a comprehensive measurement program with not only the MicroWave Radiometer (MWR) and Doppler Wind Lidar (DWL) presented in this study, but also a ceilometer and a mobile X-band weather radar, a location in a short, deep and moderately wide valley, that differs from most of the studies located in long and wide valleys.

The first objective of the campaign is to study the seasonal and diurnal cycles of T and wind in the vertical range containing the main topographical features (590-3000 m a.s.l.). The analysis is focused on both seasonality and isolated events with a deepest interest on T inversion and foehn events. A comprehensive description of along and cross valley winds is performed, including a detailed analysis of thermal winds during a heatwave event at three stations along the valley and two grid cells of the model. The second objective is to evaluate the NWP model performance (KENDA-1) used in analysis mode in the Haslital.

Comparisons with the ground-based measurements and the profiling observations allow to assess KENDA-1 performance for both monthly averages and peculiar events.

 ## 2 Methods and Data

The campaign took place in Unterbach (MEE), a secondary site in the Meiringen (MER) municipality in the Haslital valley from October 13, 2021 to August 24, 2022 in so-called complex topography. The Doppler Wind Lidar (DWL) and data from the NWP model are available during the whole campaign whereas the MicroWave Radiometer (MWR) was measuring only since end of January, ensuring however observations during winter, spring and summer months (Fig. S1 for a global view of the instrumental setup).

Unless otherwise stated, the following conventions are valid throughout the rest of the document: data are always reported by the instrument or model name and the site, e.g. MWR/MEE correspond to MWR measurements at MEE and KENDA-1/MER to modeled data from KENDA-1 at the cell comprising MER site, altitude given in meters (m) is equivalent to the altitude above sea level (m a.s.l.), wind speeds are given in km/h and direction in degrees according to north, times are in UTC format. Monthly averages are aggregated according to the median hourly values of the studied parameter, median wind speed and direction are calculated by vector averaging the hourly wind vectors.

2.1 Site

The observational site is located in Haslital, an alpine valley within the Swiss Alps in the Bernerse Oberland (Fig. 1). This 30 kilometer long valley extends from the Grimsel Pass (2164 m) to Lake Brienz (564 m). The upper southern 15 kilometers are oriented in the SE-NW direction and present a narrow valley floor with steep surrounding slopes. The Haslital is then joined by a tributary valley called Gadmertal (NE-SW) and continues towards NW with a 1.5 km wide valley floor. About 5 km after the junction, it is joined by the hanging narrow tributary valley of Rychenbachtal (SW-NE) at the Meiringen village. At this point, the valley gradually bends from NW to SW as it reaches Lake Brienz. Five kilometers before the lake, the Brünig Pass (1008 m) is an important topographic feature that connects the Haslital to the Sarneraatal, a 30 km long valley oriented in the NE-SW direction (Fig. 1 presents a detailed map of the Sarneraatal and its connection to the Haslital). This pass interrupts the near constant ridge's height around 2200 m north to the valley longitudinal axis.

The campaign provides in-situ observations from the automatic Swiss Measurement Network SwissMetNet (SMN) station at MER and REM observations from MEE facing the Brünig Pass. These two locations are separated by 4 km and are respectively at 589 and 574 m a.s.l. The main differences between these two sites are the valley longitudinal axis angle ($\phi_{MER} = 300°$, $\phi_{MEE} = 270°$) and the relative position to the surrounding connected valleys. Finally, the modelled data are available for both sites according to the existing model 1.1 km grid.
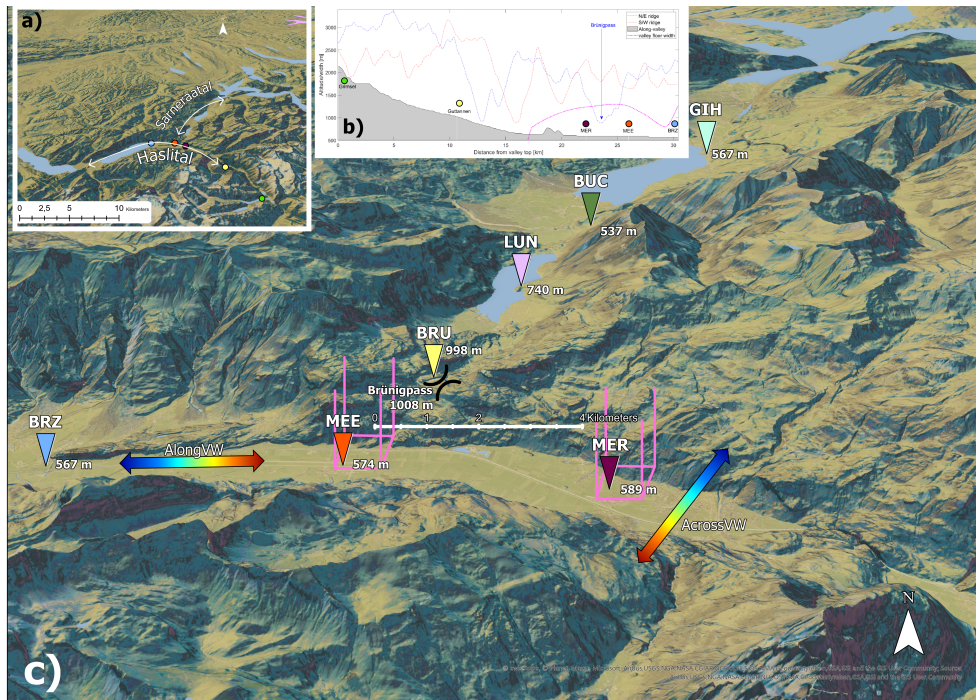
Figure 1. a) Map of the geographical situation in the lower Haslital, b) along valley altitude of the valley floor (shadowed) and of the two crests and c) a detailed view of the campaign sites, the Brünig Pass and of the ground stations in the Sarneraatal. The automatic measurement from the SMN in Meiringen (MER) is represented in purple, the campaign site in Unterbach (MEE) in red and the SMN station in Brienz in blue. The two cells of the model used are in pink. Arrows representing up/down valley winds and slope winds are colored respectively in red/blue. The map was downloaded from Swisstopo (https://map.geo.admin.ch, last access: 12.01.2024)

2.2 NWP model COSMO/KENDA-1

The NWP model used in the study is the limited-area non-hydrostatic atmospheric model from the Consortium for Small-Scale Modeling Model (COSMO) (Baldauf et al., 2011) in the operational setup of MeteoSwiss. It uses a horizontal grid size of 1.1

125 km and 81 vertical levels with spacings from 20 m at the surface, 40 m at 1000 m, to 160 m at 3000 m and coarsening further up to the model top at 22 km. The levels are terrain-following and a smooth level vertical (SLEVE) coordinate transformation is applied (Leuenberger et al., 2010).

The operational COSMO-1E forecasts are initialized by analyses produced by the Kilometre-scale Ensemble Data Assimilation system described in Schraff et al. (2016) and run in with the NWP setup of MeteoSwiss. Differences to the setup described in

130 Schraff et al. (2016) include the modeling domain (central Europe covering the Alpine Arc), the grid size of 1.1km and the observation errors tuned to the MeteoSwiss setup. KENDA-1 uses a 40 members ensemble of 1 hour model forecasts (first guess) and the following observations: SMN ground station measurements (2 m T, humidity and surface pressure), aircraft observations (T and wind from AMDAR and MODE-S), radio soundings (T, humidity and wind), and radar wind profiler (wind

speed and direction). In addition, radar-based estimates of surface precipitation are assimilated in every member using the latent heat nudging method (Stephan et al., 2008). Model first guess and observations are combined using the Local Ensemble Transform Kalman Filter (LETKF, Hunt et al., 2007) to obtain the best possible estimate of the current atmospheric state. The KENDA-1 analysis ensemble additionally uses lateral boundary condition perturbations and stochastic physics perturbations to optimize the spread-error relationship. Besides the ensemble analyses, a deterministic analysis member is calculated, which is close to the analysis ensemble mean (Schraff et al., 2016). KENDA-1 data refer to the deterministic analysis member, which are available in hourly time intervals but correspond to instant values.

Data from the two grid cells containing the MER and MEE stations were used. Both cells include part of the valley's north slope, inducing differences of 109 m and 130 m between the real topography and the model's terrain, respectively. The modeled valley floor is globally raised by a hundred meters (Fig. S2), whereas the ridges and the Brünig Pass are lowered with respect to their real altitudes. The altitude difference between the valley floor and the crests is thus reduced of several hundred meters and, in particularly, the Brünig Pass is only 200 m higher than the valley floor.

2.3 Instrumentation

2.3.1 In-situ meteorological data

The ground measurements in MER are part SMN operated by MeteoSwiss and provide every 10 minutes near real time data of T, humidity, surface pressure, precipitation amount, wind speed (mean and gust) and direction, global radiation, sunshine duration, snow height and an operational foehn index (Dürr, 2008). Surface pressure, T and relative humidity observations of the MER station are actively assimilated in KENDA-1. Anyhow, the observations considered as too far from the modeled data are rejected during the assimilation phase, so that a comparison between the observed and modeled data at MER allows making assumption on the models' skills. SMN also contains a station in Brienz (BRZ) and in the Sarneraatal (Fig. 1) in the locality of Giswil (GIH). This allows for assessing the influence of the winds originating from this auxiliary valley. MeteoSwiss also cooperates closely Federal Roads Office (FEDRO) that also operates wind measurements at the Brünig Pass (BRU), Lungern (LUN) and Buchholzbrücke (BUC) with similar temporal resolution.

2.3.2 Microwave Radiometer

A MWR (HATPRO-G5 produced by RPG Radiometer Physics Gmbh) is used to obtain T profiles by collecting microwave radiation to infer the T (Rose et al., 2005). It performs a scan every 5 minutes at 11 elevation angles and operates in 14 frequencies reception bands in two regions: 22-31 GHz (7 channel filter bank humidity profiler and LWP radiometer) and 51-58 GHz (7 channel filter bank T profiler). The device has an optical resolution of 3.5° (half power beam width) at 22 GHz. The data acquired during rainy conditions are discarded. The radiometer is measuring from 50 m above ground to 2500 m, the first MWR level is then at 625 m. The spatial vertical resolution increases from 50 m at the bottom to 300 m at the top and corresponds to a related T accuracy between 0.25 °C to 1.00 °C, respectively (Tab. S1). Löhnert and Maier (2012) found an RMSE between retrieved profiles and radiosonde data between 0.4 and 0.8 K in the lowest 500 m a.g.l., within 1.2 K at 1200 m and around 1.7

K at 4000 m above ground. However, the performance of an MWR is highly related to the retrieval algorithm and the training dataset (Rotach et al., 2015). During the Meiringen campaign, the retrieval of Payerne was used (Lohnert and Maier, 2012). This retrieval uses Payerne's radiosonde data to perform the multi-linear regression leading to potential further uncertainties. The instrument at MER had a line of sight of about 10 km inducing no further additional uncertainty due to obstacles of the surrounding terrain (Löhnert et al., 2022). In simple topography, Hervo et al. (2021) showed that the HATPRO-G5 can be still biased when compared to radio soundings with a cold bias of 0.5 K around 1500 m altitude.

2.3.3 Doppler Wind Lidar

DWL can be used to infer wind speeds and direction even in complex topography (Wang et al., 2016). During the campaign, a Vaisala Leosphere Windcube 100S DWL was deployed in MEE to measure wind speeds with a vertical resolution of 100 m. In the used measurement mode, 120 second zenith scans were performed each 10 min to measure vertical wind speed and Doppler Beam Switching scans providing 7 independent wind profiles every 5 min from 200 m to 12000 m above ground, the first DWL level is then at 775 m. Data collected during rain events or/and with confidence level < 90% are discarded. Moreover, data with wind speeds lower than 2 km/h were discarded for the wind direction analysis. The data availability during the entire campaign is of 80 % at 1000 m a.g.l. and 50% at 2500 m a.g.l.

3 Results

The measurement campaign at Meiringen allows a detailed description of the seasonality of the six months T and 10 months wind observations in the Haslital and its surroundings. Profile observations were performed at MEE and surface in-situ observations at MER, whereas the modeled surface and profile data are available at both sites. For both the T (sect. 3.1) and the wind speed and direction (sect. 3.2), the seasonality of the profile's observations and the model's performances at MEE are first described. Surface observations are than used to study specifically surface based T inversions and heterogeneity of the winds in the Haslital valley. Even if SNM/MER surface observations are assimilated by KENDA-1, the comparison of the modeled and observed data allows evaluating the impact of the assimilation at MER. Finally, a last section describes Kenda-1 performances in case of foehn events.

During the campaign, the mean T was 1°C below the 1991-2000 norm in December and January but clearly above the norm (1.5 to 2.5°C) in February, March and from May to August. Three heat waves occurred, the first one lasting 6 days in mid-June, the second lasting 4 days around mid-July and the third one reached Switzerland at the beginning of August. Snow cover and precipitation are important parameters since the surface albedo and the soil moisture affect the development of cold pools with T inversion, subsidence, the atmospheric boundary layer development and consequently thermal valley winds. Only 60% of the precipitation of the 1991-2000 norm were observed in November, but 120% in December. Snow covers the valley's floor from the end of November to mid-December. Heavy precipitation reduced then the snow cover to less than 15 cm until the end of the winter. Strong precipitation deficits happened in January and especially in March (35 and 15 mm). March experienced frequent foehn events (95 hr determined from the MeteoSwiss foehn index (Dürr, 2008)). Precipitation from May to August was 50% or

less compared to the norm, except for June (96%). The full evolution of T, precipitation and sunshine duration is aggregated in the supplement (Tab. S2 and Fig. S3) and the wind features are fully described in the results section.

3.1 Temperature

3.1.1 Seasonality of temperature profiles at MEE

The evolution of T in MEE from February to July (Fig. 2.a) presents as expected clear diurnal cycle with a vertical extent depending on the season. Layer with higher T develops gradually from sunset to sunrise to reach monthly-related maximal T and height. This layer of warmer air persists during the first half of the night and then gradually fades out towards sunrise. The time of the T maximum, the persistence of the warm layer and the T range between ground and 2500 m are all enhanced during summer months. Between the mean ridge height and 2500 m, the T remains however relatively constant throughout the day in winter (February). The maximal temporal T gradient usually follows sunrise and sunset (Fig. S4) with values up to $\pm$ 5 °C/km confined below 1500 m in the morning whereas vertical negative gradients between -4 and -6.5 °C/km are observed in the evening.

A thermal inversion layer is particularly visible from midnight to sunrise (Fig. 2.a) near the ground (590-1000 m) for all months in the study. The frequency of occurrence of these T inversions are highlighted by the positive vertical T gradient. A complete analysis of T inversion will be described in section 3.1.3.

Fig. 2.b presents the differences between the observed MWR/MEE and modeled KENDA-1/MEE T profiles. The main observed pattern is a general low altitude (< 1500 m) T underestimation from KENDA-1/MEE. In February, this underestimation lasts almost the whole day up to 2500 m, but is larger (< -1 °C) below 1500 m. March and April exhibits the same T underestimation below 1500 m, while a small T overestimation (< 1 °C) is also observed in March over the ridges in the morning. In May and June, underestimations are constrained to nighttime. July also exhibits lower altitude (< 1000 m) T underestimation but also a near continuous T underestimation of up to -2°C at ridge level, that was already partly present in May and June. The 1-2°C underestimations of KENDA-1/MEE models are then slightly larger than the MWR uncertainties comprised between 0.25 and 1°C as a function of altitude (see sect. 2.3.2). The cold bias between the MWR and the radio sounding could however suggests a larger error of KENDA-1.

3.1.2 Surface temperature comparisons

To better estimate the reliability of the REM observations and of the model, the first levels of MWR/MEE, KENDA-1/MEE and KENDA-1/MER are compared to the SMN/MER measurements used as a reference due to its low uncertainty ($\approx$ 0.2 °C). The T differences between MWR/MEE and SMN/MER (Fig. 3.a) are normally distributed with mean and median close to zero (-0.07°C) and RMSE equal to 1.45°C. Extreme differences (3σ) are larger than $\pm$ 4.35 °C.

The distribution of ground T differences between KENDA-1/MEE and SMN/MER (Fig. 3.b) is wider than for the MWR/MEE (RMSE = 2.23 °C) and exhibits a positive skew (median = -0.27 °C and mean = +0.03 °C). Extreme values are significantly more frequent than for the MWR/MEE measurements, especially in the positive part of the distribution. KENDA-1/MEE T
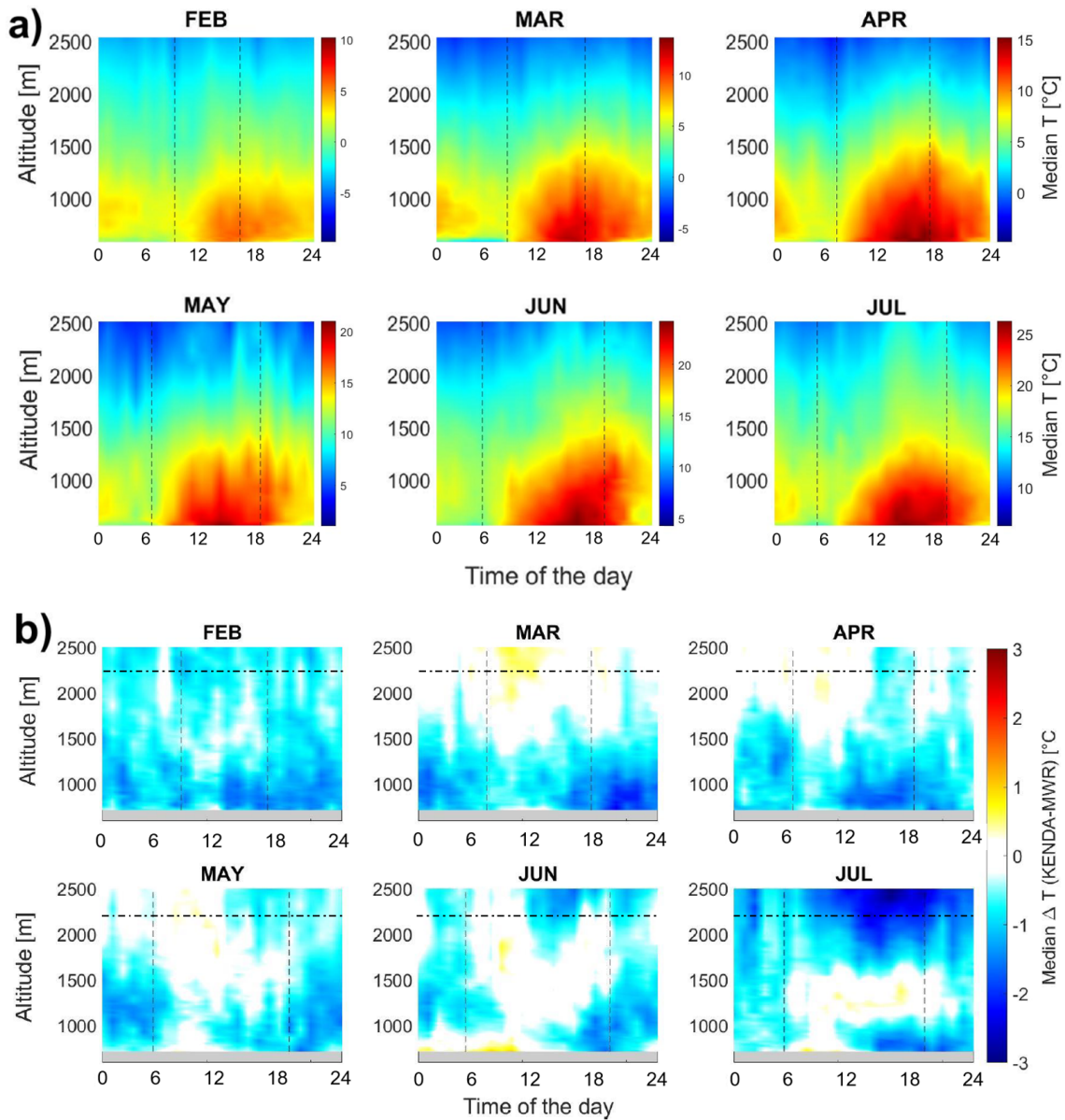
Figure 2. a) Monthly diurnal cycle of MWR/MEE T from February to July 2022. Monthly scales with a range of 20 °C but with minimum T based on the MWR/MEE profiles are used. b) Diurnal cycle of the median T profiles difference [°C] between KENDA-1/MEE and MWR/MEE for each month. The dashed vertical lines correspond to sunrise and sunset times and the dashed horizontal line to mean ridges' height.

230   underestimations occur more often but with lower absolute differences than overestimations, and differences with the SMN/MER T reference can reach up to 9 °C. A similar distribution is observed for KENDA-1/MER (Fig. 3.c) with the same occurrence of
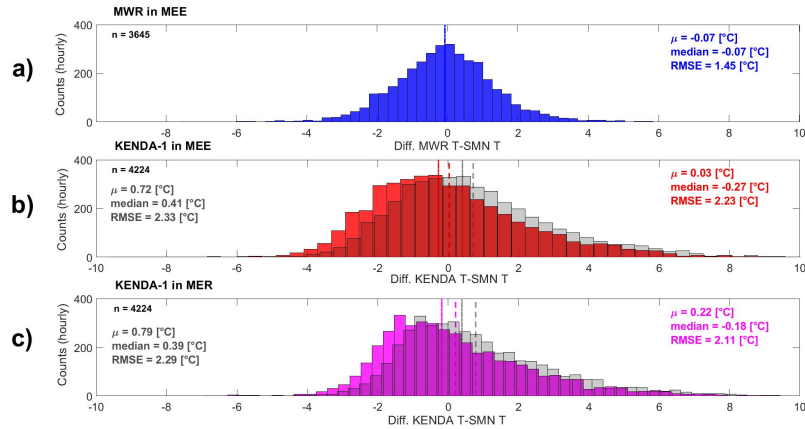
Figure 3. Distribution of the ground hourly T differences for a) MWR/MEE-SMN/MER b) KENDA-1/MEE-SMN/MER, c) KENDA/MER-SMN/MER. The gray distributions are the ground T differences with ELR corrections. The dotted and dashed lines correspond to the median and the mean, respectively.

extreme T differences (217 hr). Differences under 2 °C represent 71.1 % at MER and 66.0 % at MEE which explains the slightly smaller RMSE for the cell over the SMN station.

To check if the altitude differences between the stations and KENDA-1 first levels could explain the T differences with
235   SMN/MER, a standard T correction with a mean environmental lapse rate (ELR) (-6.5 °C/km (Lute and Abatzoglou, 2021)) close to the mean measured MWR/MEE lapse rate (-4.59 °C/km between 590 and 740 m) was applied to the modeled profiles. Considering the remaining T differences after the correction (grey in Fig 3.b and 3.c), we conclude that the horizontal and vertical distances between the SMN/MER station and the first level of KENDA-1/MEE are not the main causes of discrepancies in ground T estimation.

240   The median diurnal cycle of T differences with SMN/MER T (Fig. 4) shows that KENDA-1 overestimates the T during nighttime (+1.5°C) in both cells and underestimates it during the day (-2°C in MEE and -1.5°C in MER). The interquartile range (0 to 3.5 °C) and the whiskers (-4 to 8 °C) of the differences are larger during the second part of the night for KENDA-1 when surface T inversions are more frequent. The presence of this phenomenon strongly influences the amplitude of the differences (see details in next section 3.1.3). One third of the daily bias can be explained by the altitude difference between the
245   station and the KENDA-1 first level since the median T correction during daytime is around 0.65°C. The T bias distribution of KENDA-1/MER and KENDA-1/MEE are similar during most of the cycle. The modeled daytime T over MER shows however smaller differences to SMN/MER than over MEE, which can be explained by the reduced altitude bias or the reinforced assimilation. MWR/MEE also has a negative T bias (> -1°C) from 6:00 to 15:00 followed by a slight overestimation from 15:00 to 21:00 (< + 0.5 °C). The MWR/MEE T differences present smaller whiskers and interquartile range during the second part of
250   the night than KENDA-1/MEE, but they are similar during daytime. Globally, the measured MWR/MEE first level T are closer to the SMN/MER T than the modeled T.
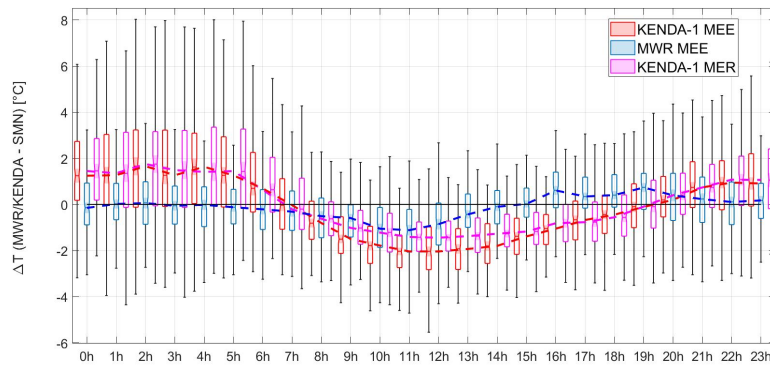
Figure 4. Box plots and whiskers of hourly ground T differences between the SMN/MER and the MWR/MEE (blue), the SMN/MER and KENDA-1/MEE (red), the SMN/MER and KENDA-1/MER (pink) as a function of daytime. The dashed lines represent the median of the distributions.

3.1.3 Surface temperature inversion

A comparison between the T inversions detected by two ground observations at different altitudes (MER and BRU), by REM MWR/MEE and modeled by KENDA-1/MEE allows a better estimation of the frequency of occurrence of cold pools, the
255 sensitivity of REM observations and the limitations of the model.

The analysis of the negative ground T difference between MER at 590 m and BRU at 998 m (horizontal distance = 3.7 km) shows that near ground T inversions are common during the night for all months in the study (Fig. 5.a). Their frequency is 60% in December and January (all day long), 40% during spring nights and 30% during summer nights. Daytime near ground inversions are rare from March onwards and common between November and February (20-60%). The observed T inversion
260 amplitude follows a seasonal cycle with stronger inversions during winter months reaching up to 4 °C (Fig. 5.b). In summer, this amplitude is reduced to about 2°C and constrained to nighttime. The erosion speed of the T inversion is independent of the month. However, the delay of the erosion onset to sunrise is smaller in summer (about 2h) than in winter (about 4h).

The same analysis between two similar elevations is performed on MWR/MEE and KENDA-1/MEE T profiles. MWR/MEE shows higher frequencies of T inversion than both the ground stations and KENDA-1/MEE, especially for June and July.
265 MWR/MEE also presents a larger amplitude of the T inversion than the ground observations and KENDA-1/MEE with maximum difference of +2°C and +4°C, respectively. Even if the capability for KENDA-1/MEE to detect the near ground T inversions is enhanced from November to January, their amplitude is always underestimated by 1-2°C (Fig. 5.b). Moreover, from May to August, the presence of T inversion in the first hours after sunrise is also underestimated by KENDA-1/MEE, which can impact the onset time of up valley winds (section 3.2.2). The missed T inversions by KENDA-1/MEE leads to both its important
270 overestimation of the T at ground level (Fig. 4) and its slight T underestimation between 850-1200 m (Fig. S5 for detailed examples).
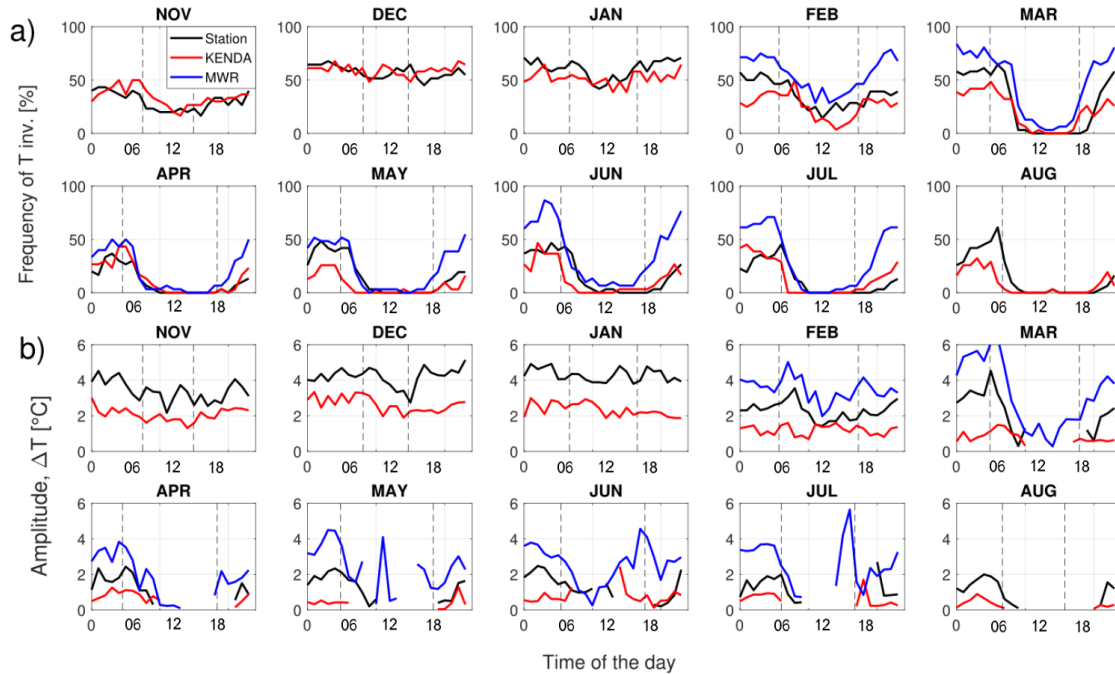
Figure 5. a) Diurnal cycle of the hourly T inversion frequency between T at SMN/MER (589 m) and FEDRO/BRU (998 m) ground stations, at the lowest level (640 and 705 m, respectively) and 1000 m of MWR/MEE and KENDA-1/MEE profiles. The 1D measured values were interpolated using a linear interpolation with 10 m spaced vectors. b) Mean ΔT for the time where an inversion is detected. Sunrise and sunset are represented by dotted lines.

The analysis of the assimilation process for nights with strong ground KENDA-1/MER T overestimations shows that the model suffers from a systematic deficiency. During these nights, differences between the model's first guess and observations are mainly around 5 °C and can reach 10 °C in extreme cases (results not shown), so that observations are rejected due to differences exceeding the predefined threshold based on the ensemble first guess, its spread and the observation error. During these periods, the SMN/MER T is therefore not assimilated by the model analysis. Even if the observations are assimilated for some of the KENDA-1 time steps, the assimilation has a very limited effect and allows only minor corrections towards the observations (< 1 °C) during some nights in both MEE and MER. It has to be noted that the KENDA-1 T overestimation during nighttime is similar at MEE and MER (Fig. 4).

3.2 Wind

During the campaign, wind profiles were measured at MEE by the DWL, whereas ground based 10 m wind compounds are constantly measured at MER and at five other SMN or FEDRO ground stations (Fig. 1). Modeled wind profiles from the two grid cells of MER and MEE are further used. The average measured wind profiles' seasonality is first described followed by a more detailed analysis of the along and across valley components at MEE. The performance of KENDA-1/MEE is analyzed

in each section. A comparison between the results in MEE and in other ground stations in the valley gives an insight in the complexity of the wind system caused by the peculiarities of the valley's topography.

3.2.1 Seasonality of wind profiles at MEE

For the monthly average of DWL/MEE and KENDA-1/MEE profiles, wind directions are split into two speed categories, below and above 20 km/h, to distinguish between thermally induced valley winds and external synoptic winds, respectively. Fig. 6.a presents the monthly mean wind directions from the DWL/MEE observations.

Concerning thermally induced winds ($w_s < 20$ km/h), winter months do not show a clear presence of regular direction changes at any altitudes. A predominance of easterly winds is measured in January and February at low altitudes. During March, despite the channeled easterly winds due to frequent foehn events, the formation of valley winds pattern is already clearly visible. Their time extent from mid-day to sunset is similar to November. The formation of thermally induced wind is clearly visible from April to August ($w_s < 20$ km/h) and will be further discussed in the next section (3.2.2). From 10:00 to mid-afternoon, the direction at low altitudes (800-1000 m) is mainly from W-SW, whereas flows from W-NW are measured in the rest of the profile concerned by up valley winds (see further explanation in sect. 3.3). Synoptic winds ($w_s > 20$ km/h in Fig. 6.a) are measured between 2000 and 3000 m from W-SW direction for all months, with a higher variability in January and a strong influence of foehn events up to 2500 m in March. In December and February, high speed winds from W-NW are prevalent below 1500 m whereas various directions from N to SE directions are observed for the others months. From April to November, high speed N winds from Sarneraatal (sect. 3.2.3) are also observed from the ground to 1000-1500 m from the late morning to several hours after sunset.
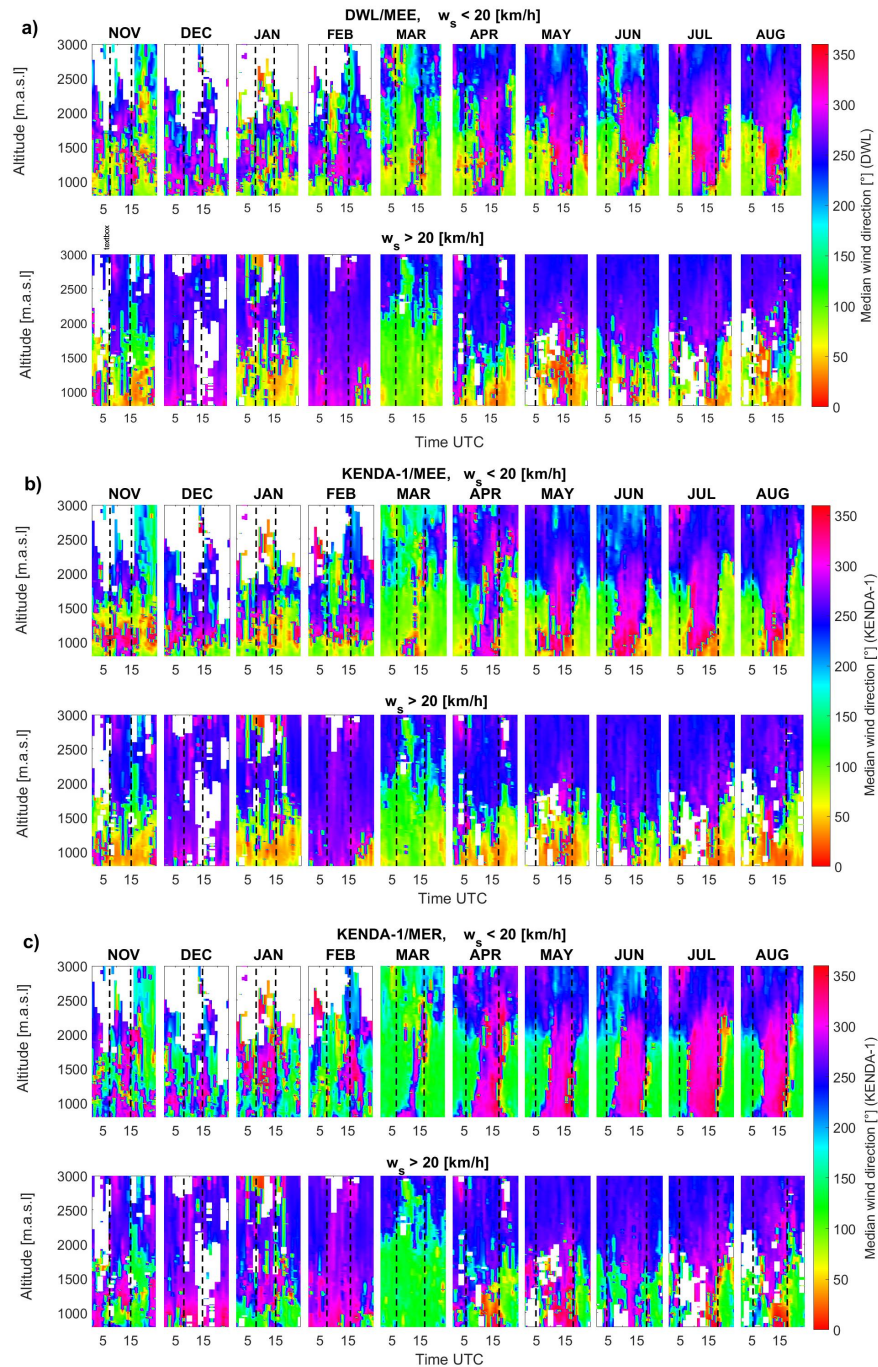
Figure 6. Monthly median wind direction [°] for a) DWL/MEE, b) KENDA-1/MEE and c) KENDA-1/MER (01.11.2021-23.08.2022). In each case, the data are split according to the threshold wind speed of 20 km/h.

KENDA-1/MEE wind profiles (Fig. 6.b) are generally very similar to the DWL/MEE observations. The good KENDA-1/MEE performances comprise first the influence of the foehn up to 2500 m ($w_s > 20$ km/h) as well as the presence of valley wind below 1200 m ($w_s < 20$ km/h) in March. Second, the synoptic wind flows ($w_s > 20$ km/h) captured by large grid model inputs and by assimilated measurements (e.g. RS, MWR and DWL profiles) from the Swiss plateau are consequently very well modeled. Finally, the main valley wind patterns in November and from March onwards are well represented by KENDA-1/MEE. Apart from inaccuracies related to the valley wind transitions (see 3.2.2), the model and the measurements differs in the presence of frequent N flows from the Brünig Pass between the ground and 900-1200 m with increasing frequency towards sunset in KENDA-1/MEE, whereas N flows are rather found at higher altitude (1300-1700 m) in DWL/MEE. This feature is mostly caused by the KENDA-1/MEE cell overlapping the slope towards the Brünig Pass so that winds at the junction between Haslital and Sarneraatal can influence the median modeled wind compounds. Finally, during winter months, KENDA-1/MEE models continuous down valley (E) winds ($w_s < 20$ km/h) between ground and 1000 m that are less continuously observed by the DWL/MEE in January and February and even absent in December.

3.2.2 Along valley winds

To extend the wind analysis, the data from the SMN/MER station, the DWL/MEE and KENDA-1 at MEE and MER are transformed according to the valley longitudinal axis directions at both sites. For this analysis, the positive wind speeds (red color) correspond to up valley wind (Fig. 1) and to northern wind from the Brünig Pass for along and across valley winds, respectively, and negative wind speeds (blue color) to opposite directions.

Fig. 7.a shows the diurnal and seasonal cycles of the along valley wind speed at SMN/MER during the campaign. The occurrence of along valley winds is confirmed by the diurnal cycle in November and from February to August. A 3-4 hours delay between sunrise and the onset of up valley winds (> 10 km/h) is observed. February shows some early up valley wind but their origin is more linked to synoptic flow intrusions. The transition to down valley winds occurs 1 hours before sunset in March and June and around sunset otherwise. The maximum median up valley wind speeds are between 15-20 km/h. Down valley winds are weaker with a median maximum speed of 2-7 km/h reached within the 2 to 3 hours after sunset. These results are in good agreement with the 10-year climatology (Fig. S6), which presents however a clear wind speed maximum in July and an onset of down valley winds 1-2 hours after sunset in spring.

Similar diurnal and seasonal cycles of the valley wind at the first level are measured by the DWL/MEE at 775 m (Fig. 7.b). The onset of the up valley winds occurs with the same delay to sunrise (4 h) during the summer months but their speed is of reduced maximum amplitude (10-15 km/h) than at SMN/MER. At 775 m, the up valley wind intensity is also less regular than at ground with maximum speed around noon for May to August. The strongest down valley winds are also measured in the first part of the night, with a higher wind speed (5-10 km/h) compared to the ground at MER. Additionally, during August, down valley winds occurring two hours before sunset are observed by the DWL/MEE whereas the onset to down valley winds occurred just after sunset at SMN/MER (Fig. 7.a), a difference linked to the presence of the Brünig Pass (sect. 3.3).

Overall, KENDA-1/MEE shows similar results as the DWL/MEE (Fig. 7.d). The modeled valley winds evolution is consistent with the measurements, including the presence of turbulence leading to daytime varying wind direction. The main differences
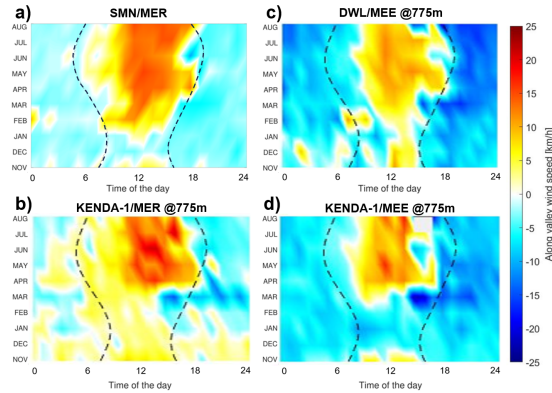
Figure 7. Monthly evolution of along-valley wind speeds [km/h] a) observed at the SMN/MER, b) observed at MWR/MEE, c) modeled at KENDA-1/MER and d) modeled at KENDA-1/MEE. Sunrise and sunset are represented with dashed lines.

are a slightly higher up valley wind speed, an underestimation of the down valley winds speed and an earlier onset of up valley winds. The comparison of the first level of KENDA-1/MER (Fig. 7.c) and SMN/MER (Fig. 7.a) indicates an underestimation of thermally induced along valley wind by KENDA-1/MER, which leads to the absence of diurnal cycle in November and December. Even in summer months, the along valley wind diurnal cycle is less pronounced in KENDA-1/MER due to the presence of weak up valley wind in the second part of the night. The modeled data at MER and MEE also present marked differences, principally a stronger presence of up valley wind during the whole campaign leading to stronger maximum up valley and weaker down valley wind speeds and the presence of weak up valley wind during all day in winter.

The monthly diurnal cycle of DWL/MEE wind profiles (Fig. 8.a) allows a better visualization of the vertical extent of valley winds. First, the height of the down valley wind determines the limit of the influence of SW synoptic winds. Thermally induced wind height increases with temperature, reaching 1000 m in February, 1800 m in May and up to 2000-2200 m in July and August. The clear influence of synoptic winds reaches then ∼ 1500 m in winter, 2000 m from April to June and 2500 m in July and August. Second, the onset of up valley wind occurs simultaneously over the full valley wind extent 3-4 hours after sunrise, whereas the onset of down valley wind is delayed from ground to its maximal extent. Up valley wind can then persist until 1-3 hr after sunset at the ridge's height. Third, down valley wind speed decreases with altitude and with time after sunset. Finally, the daytime wind direction between 1000 m and 1500 m does not stay constant even during summer months. This might be related to potential turbulence in valley wind regimes (Krishnamurthy et al., 2011), especially when synoptic flows interact with thermally driven flows, or to influence of flows from the Sarneraatal. In spring and summer, the up valley winds are stronger and more uniform at 1500 m than at 1000 m and persist longer in the afternoon probably under the influence of the synoptic winds.

The same representation for KENDA-1/MEE (Fig. 8.b) shows that the vertical extent of the modeled valley wind is comparable to the observation (± 100 m) except in April, when KENDA-1/MEE modeled a much stronger and higher wind diurnal cycle. The main differences are, first, an underestimation of the down valley wind speed from ground to 1600 m until midnight in summer and, second, a 1-2 h too early onset of up valley winds after sunrise between the ground and 1200 m. Third, in

November, the modeled profiles show continuous up valley winds between 1000 and 1700 m where the DWL/MEE measures

360 mostly down valley winds. Finally, KENDA-1/MEE overestimates the influence of the synoptic winds leading to the absence of along valley wind in winter replaced by constant slow down valley winds below 1200 m and to higher up valley wind speed in spring and summer. The foehn influence in March up to 2500 m is on the contrary well modeled.
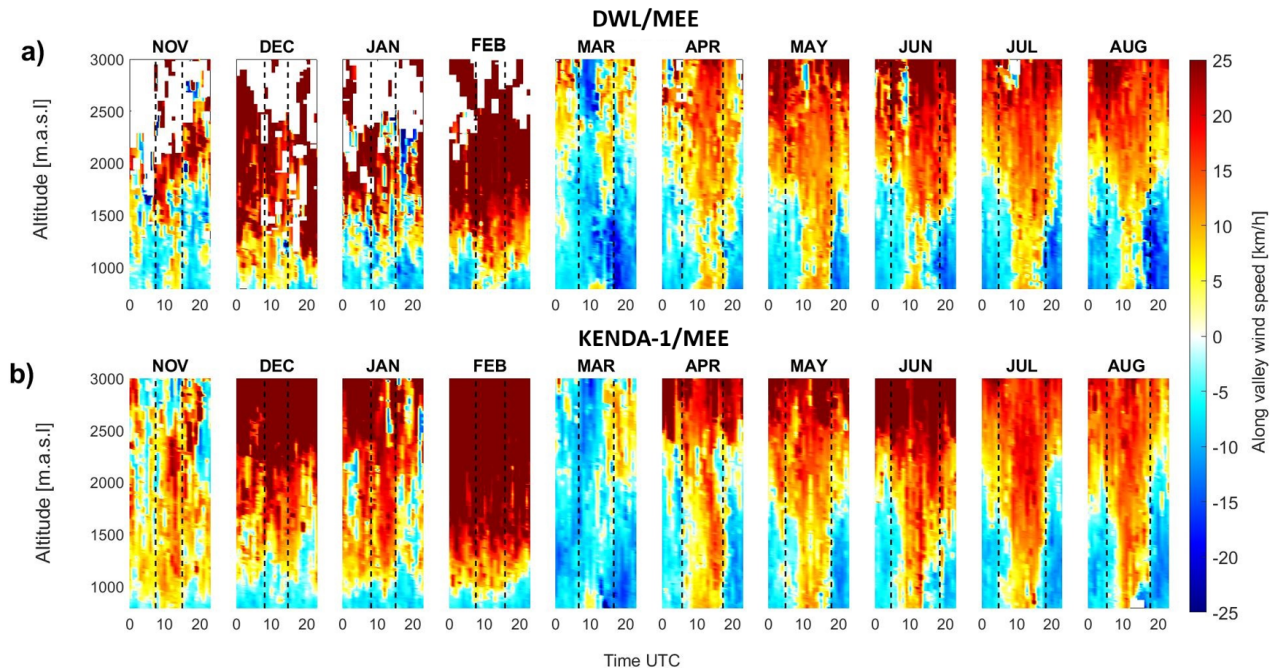
Figure 8. Monthly diurnal cycle of the along-valley wind component [km/h] as a function of altitude for a) the DWL/MEE observation and b) the KENDA-1/MEE data. Sunrise and sunset at ground level are given by dotted lines.

3.2.3 Cross valley winds

The cross-valley winds at MEE can originate from thermally induced slope winds in the Haslital or from valley winds from the

365 Sarneraatal passing over the Brünig Pass. Fig. 9.a shows the monthly diurnal cycle of the cross-valley wind measured by the DWL/MEE. During winter, the data are scarce and no particular pattern is visible except the presence of Brünig Pass N winds from 800 m to 1500 m in January and February. During all other months, strong cross valley winds originating from Brünig Pass start between midday and sunset and stop around midnight. They are generally first measured near the ground and reach 1200-1500 m after sunset, where they reach wind speeds of 20-25 km/h and can extend up to 2500 m with weaker speed. These

370 intense north-facing slope winds (> 25 km/h) are also observed between 1400 and 2000 m during some hours around sunset with a much lower intensity in May. This suggests a circular motion with North updraft winds (median vertical velocity of 1 km/h) that cross the valley at a low altitude, rise against the north facing slope and come back at higher altitude with a South

downdraft component (median vertical velocity of -2 km/h). Plots of radial winds perpendicular to the valley direction clearly present this circulation pattern both in presence of up and down valley winds around sunset (Fig. S9).

375   KENDA-1/MEE also shows cross valley wind patterns (Fig. 9.b) with strong winds from Brünig Pass from March to August. These N winds also develop progressively from ground to 1400 m and stop around midnight. They are however modelled earlier than measured, at the time (10:00) of the onset of up valley winds in the Sarneraatal. Winds from the north facing slopes between 1400 and 1800 m are never modeled by KENDA-1/MEE despite their intensity and being systematically measured from April to August. The influence of the Sarneraatal wind on the thermal wind system in the Haslital is not only visible near the ground but

380   also in the difference between the modeled wind profiles at MER and MEE. The along valley diurnal cycle is more pronounced at MER with more constant up valley wind direction at 1000 and 1500 m and higher down valley wind speed, particularly in the morning at 1500 m. KENDA-1 also modeled a lower influence of synoptic winds at MER than at MEE, with almost no at 1500 m even during winter and less influence event at 2500 m in summer. These modeled differences between the two cells can be explained by the different orientation of the valley at both sites and by a already discussed vanishing influence of flows from the Sarneraatal at MER.
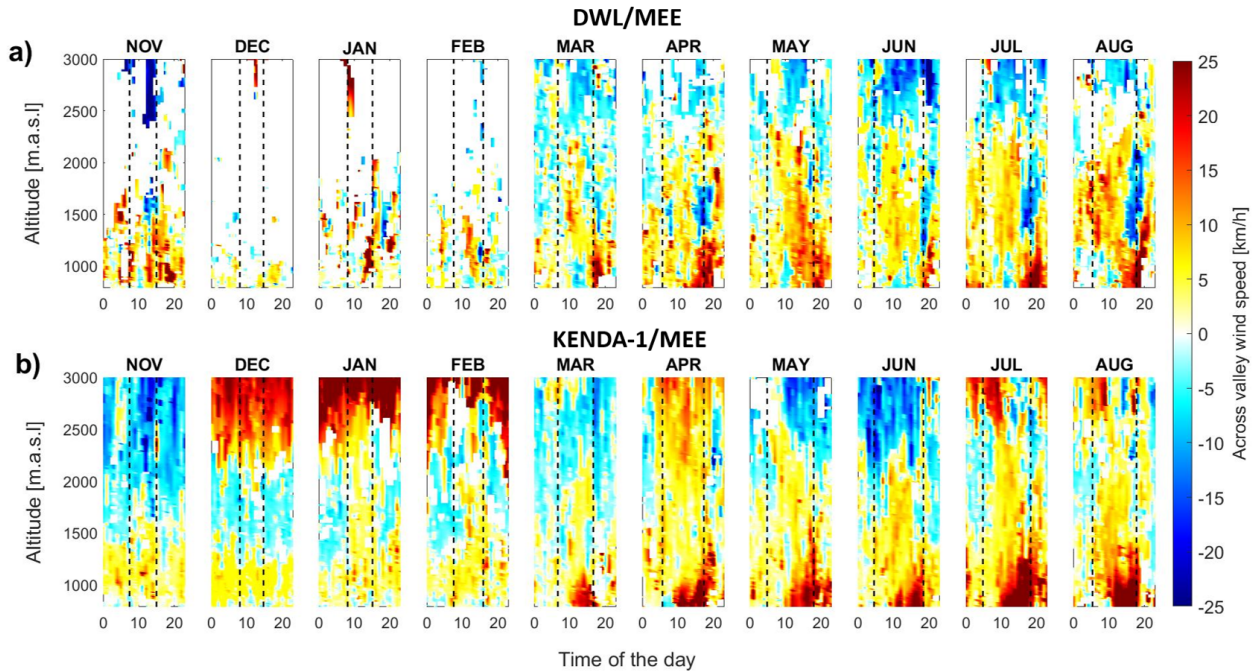
Figure 9. Evolution of the diurnal cycle of the cross-valley wind component [km/h] as a function of altitude for a) the DWL/MEE measurement and b) the KENDA-1/MEE. Winds coming from the south-facing slopes take a positive value (red), for the north-facing slope wind speeds values are negative (blue). Sunrise and sunset at ground level are given by dotted lines.

385

3.3 Heterogeneity of wind patterns in the Haslital

The design of the Meiringen campaign requires us to compare modeled data to observations at two different sites with different valley directions and different topographic features. The presence of additional wind ground observations in the Haslital and in the Sarneraatal allows a detailed analysis of the effect of the Brünig Pass during clear summer days. The modeled data allow some further insight in the difference of the thermal wind system at MER and MEE in the entire valley volume.

A closer look at the SM/MER and DWL/MEE wind speeds during a series of clear warm days in July with low cloud coverage (Fig. 10) shows some particularities relative to the previous analysis of along valley wind on the basis of a monthly median values. In MER (Fig. 10.a), a clear diurnal pattern of thermally induced winds is measured. The onset of up valley winds occurs at 10:00 and the wind speed strengthens during the day (approximately +4 km/h per hour) to reach a maximum of 25-30 km/h at 15:00-16:00. The onset of down valley winds occurs at 19:00. During night, down valley winds are constant in direction and drop to 0-5 km/h. It has to be mentioned that the direction of up valley winds at MER gradually shifts from the longitudinal axis of the Haslital towards an enhanced northern component on the 10 and 11 July during the afternoon.

At the DWL first level (200 m a.g.l.), up valley wind is only measured in DWL/MEE on the 10 July at 13.00-14:00 (Fig. 10.a, color bar). The wind direction switches thereafter to N and the wind speed increase gradually to reach 40 km/h at 20:00. The wind then weakens until midnight and changes direction afterward with a down valley wind direction that persists occasionally (e.g. on the 12 July) during the morning. Along valley wind patterns following the valley longitudinal axis (W/E) are only observed between 1300 m and 2000 m (not shown), namely higher than the Brünig Pass altitude. They then present a standard diurnal cycle with up valley wind measured from 09:00-10:00 to 16:00-17:00 with wind speeds between 15 and 20 km/h.

In BRZ, the wind pattern varies during the three selected days (Fig. 10.a). July 10 and 12, up valley wind begins at 8:00 and last until 14:00 with low wind speeds between 5 and 10 km/h. At 14:00, the wind direction switches towards down valley winds (17-19 km/h), which last until 20:00. A small direction change towards WSW occurs during the night. July 11, there is no up valley wind phase with only down valley wind (NE/N). The wind speeds are lower in the morning and strengthen to 20 km/h in the afternoon before to drop at 21:00.

The strong influence of the thermal winds from the Sarneraatal over the Brünig Pass during hot summer days is highlighted by this wind analysis at the three stations. An analysis of ground measurements from the BRZ, BRU, LUN, BUC and GIH (Fig. S8) automatic stations shows that flows measured at the Brünig Pass switch towards the Haslital (SSW) 2 to 3 hours earlier (5:00-6:00) compared the onset of up valley wind at other stations in the Sarneraatal (08:00-09:00) and last much longer after sunset, up to 21:00-22:00. These winds from the Brünig Pass explain first the N wind observed in MEE during the afternoon, the early evening and even sometimes in the morning (e.g. on the 11 of July). Second, they also strongly influence the diurnal cycle at BRZ leading to the onset of down valley winds in the early afternoon or even by suppressing up valley winds (July, 11). Finally, their influence at MER is weak with only a slight shift of the wind direction towards N in the late afternoon. During these summer days, a standard thermal wind diurnal cycle is observed in MER and in MEE at altitudes higher than the Brünig Pass (not shown).

Concerning the modelled data (Fig. 10.b), the influence of the Sarneraatal thermal winds is well captured by KENDA-1/MEE so that the differences between MER and MEE are important. At MER, the wind speeds and direction follow a clear thermally driven valley wind diurnal cycle whereas a relatively stable wind direction from NE during nighttime and NNE during daytime is modeled at MEE. Speeds at MEE are always equal or higher than over MER with weaker diurnal cycle. The major differences compared to the observations are an overestimated influence of the valley winds from the Sarneraatal leading to no modeled down valley winds at MEE during the night and the morning as well as a shift in wind direction toward N at MER. The differences of the wind speed diurnal cycles at MER and MEE are well modeled by KENDA-1, but the wind speed is overestimated at both sites with differences up to +30 km/h.
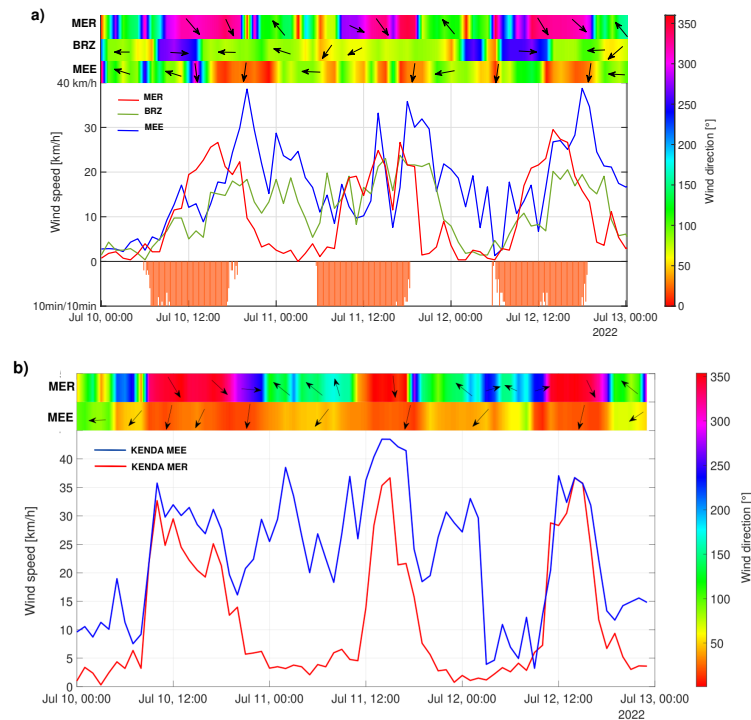
Figure 10. a) Measured b) modeled wind speeds (solid lines), wind direction (colored bands and arrow) and sunshine duration (orange bars) for a) the DWL/MEE (800 m), the SMN/BRZ, the SMN/MER and b) KENDA-1/MEE (800 m) and KENDA-1/MER (800 m).

Strong heterogeneities in the wind pattern along the Haslital valley are not only observed in this detailed analysis of thermal wind during summer time but also in the previous analysis of median monthly wind. The comparison of KENDA-1/MER and KENDA-1/MEE (Fig. 6 b and c) wind profiles, confirms the perturbation of the thermal wind diurnal cycle in the Haslital by the Sarneraatal winds. In MER, the influence of up valley winds is more pronounced with a clear extension up to 2000 m in November, March and April, a more delayed onset as a function of altitude in spring and a less turbulent and more constant wind direction during all months (Fig. 7). Generally, the onset of down valley wind is better defined in MER due to the absence of

winds from the Sarneraatal. It has to be noted that up valley winds modeled at MER take almost the same direction (300-310°) as at MEE (290-300°), even if the valley bends (≈ 30°) between the two sites, except in the early morning (sunrise to 10:00) when up valley winds come from W at low altitude (from MEE direction). This near ground direction difference is similar to the observed winds at MEE, but happens earlier (from sunrise) and disappears at 10:00. Modelled down valley winds in MER always follow the main longitudinal valley axis, like in MEE.

3.4 Foehn events

Foehn is a katabatic wind bringing strong warm and dry downdraught usually leading to clear weather conditions. The study of the T during foehn events combines all the periods where foehn was measured at the SMN station in MER, according to the foehn index. The study on the wind is however performed on only three selected events (10-16 March 2022/19-22 March 2022/26-24 April 2022) representing 117 hours of foehn during clear weather in March, while the April and June episodes presented a slightly overcast sky (50-70% of maximum global radiation).

3.4.1 Temperature during foehn events

During foehn events, the MWR/MEE tends to measure 0.5-1.5°C lower T than the SMN/MER (Fig. 11.a), which can be partially explained by the different sites locations and altitudes. In contrast, a significant KENDA-1/MER and KENDA-1/MEE T underestimation of -2 to -4 °C is observed regardless of time of day. Furthermore, the differences categorized according to measured wind speed (Fig. 11.b) show that larger wind speeds (> 20 km/h) induce larger median T underestimations. Saigger and Gohm (2022) performed simulations in the Inn valley with the Weather Research and Forecasting model and observed similar bias at low altitudes during an intensive foehn event. Additionally, Tian et al. (2022) also report significant cold and moist biases in the model during foehn hours. Note that the KENDA-1/MER is in better agreement than KENDA-1/MEE with SMN/MER (not shown), which can indicate significant differences in the foehn influence at the two stations.

The comparison of T profiles during foehn events in March (Figs. S11 and S12) shows that KENDA-1/MEE and KENDA-1/MER underestimates the T not only at the surface but up to 900-1400 m depending on the event. In some cases, KENDA-1 missed the T increase due to foehn but in other cases, KENDA-1 follows the T evolution but with a smaller T gradient. The median T bias of 2-4°C observed at the surface is also measured along the profile and is reinforced when a T inversion missed by KENDA-1/MEE precedes the foehn event. The T increase due to the foehn breakthrough measured by the MWR/MEE is delayed by less than one hour compared to the SMN/MER detection. Similar time delays of about one hour are modelled by KENDA-1, with shorter delay at MER than at MEE as expected by the orientation of the Haslital and the provenance of foehn.

3.4.2 Wind

DWL/MEE measurements (Fig. 12.a) shows the extend of the higher wind speeds induced by the foehn from ground to the ridge's height (1800-2000 m) for a selection of three cases in March and April 2022. The foehn breakthroughs are nearly simultaneous at ground (SMN/MER) and up to 1000-1500 m at DWL/MEE for the events of March 11 and April 23. For March
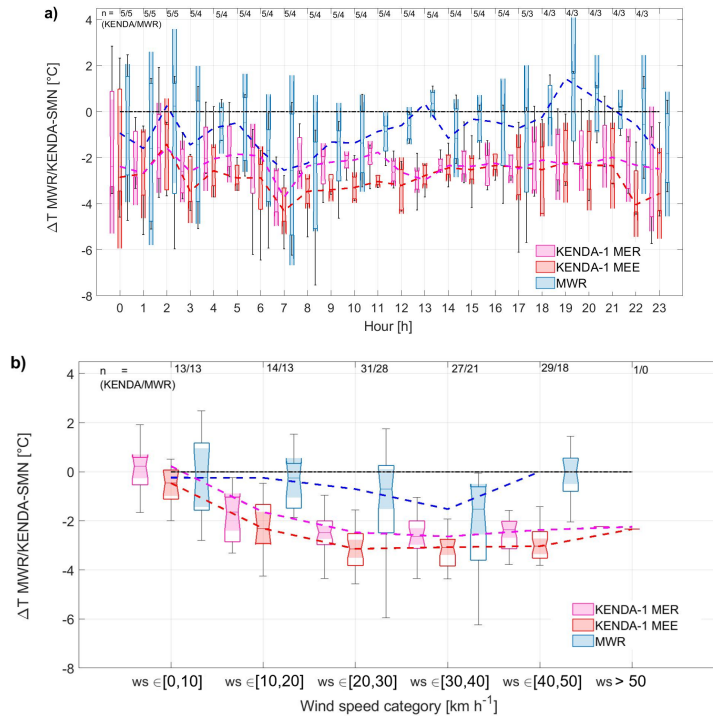
Figure 11. Box plots and whiskers of ground T differences between MWR/MEE and SMN/MER (blue), KENDA-1/MEE and SMN/MER (red) and SMN/MER and KENDA-1/MER (pink) as a function of a) the hour of the day and b) the 10 m measured wind speed at SMN/MER for all foehn events during the campaign. The dashed lines represent the median of the different distributions and n is the number of cases in each of the categories.

20, an important delay of ≈ 3 hr is measured between 800 and 1300 m, whereas foehn winds are measured from 1300 m up to
465   the ridge at the same time as at SMN/MER. The maximal measured wind speeds at 800 m in DWL/MEE (60-75 km/h) are higher than at the SMN/MER (45 km/h), especially for the event of March 11.

    During the first selected episodes (11.03) the foehn arrival is modeled 2 hr too early by KENDA-1/MEE (Fig. 12.b) with strong winds (60 km/h) from SE between 800 and 1000 m. After the foehn breakthrough (11:00), the KENDA-1/MEE wind direction is coherent with measurements but wind speeds are first overestimated by 15-30 km/h between ground to ridges height
470   during 4 hr (Fig. S13), then underestimated during 2 hr before being in accordance with measurements for the rest of the event. For KENDA-1/MER (Fig. 12.c), the same premature onset in the foehn breakthrough is observed but over a larger vertical extent (800 to 1200 m) and with even higher wind speeds (> 100 km/h) lasting during the entire event.

    During the second episode, KENDA-1/MEE models correctly the 3h delay between SMN/MER and DWL/MEE measurement (Fig. 12.b) but extends it up the ridge height contrarily to the measurements. The KENDA-1/MEE wind speeds tend to be
475   overestimated (+15 km/h) from ground to 1100 m during the entire event and underestimated from 1100 m to the ridge's height

(-30 km/h) the first hours following the breakthrough. KENDA-1/MER modelled again wind speeds up to 100 km/h with a foehn breakthrough at the same time as the SMN/MER (Fig. 12.c). At the very end of the event (March 20 at 23:00), KENDA-1/MEE and KENDA-1/MER keep showing foehn winds between 900 and 1500 m while no wind is measured (SMN/MER and DWL/MEE).

480 Few DWL/MEE measurements are observed during the third selected episode, but the timing of the foehn breakthrough and the wind speed are similar at SMN/MER and DWL/MEE. The breakthrough is modeled with a long delay by KENDA-1/MEE but almost in time by KENDA-1/MER and the end of the foehn episode is also delayed by both KENDA-1/MEE and KENDA-1/MER. The wind speed is also overestimated if compared to SMN/MER, particularly by KENDA-1/MER with maximum speed higher than 75 km/h during the whole event.

485 To summarize, the three analyzed events exhibit some similarities but also large differences. The foehn breakthrough is often observed some hours later by DWL/MEE than by SMN/MER and not always simultaneously in the entire profile. The wind speed at the DWL/MEE first level is usually similar to the one at SMN/MER. KENDA-1 tends to model the foehn arrival and end with positive or negative time shifts at both stations. The most critical point concerns the very high KENDA-1/MER modeled speed up to 110 km/h from ground level to 1500 m that is twice faster than the DWL/MEE observation, 5 km further down in the valley. Even though the Haslital is narrower just before MER, such wind speeds difference is subject to a discussion
490 about a potential large overestimation of the winds at this location. Finally, the simultaneous wind speed overestimation and the T underestimation by KENDA-1 during foehn events are difficult to explain since a stronger foehn should allow for a greater T increase.
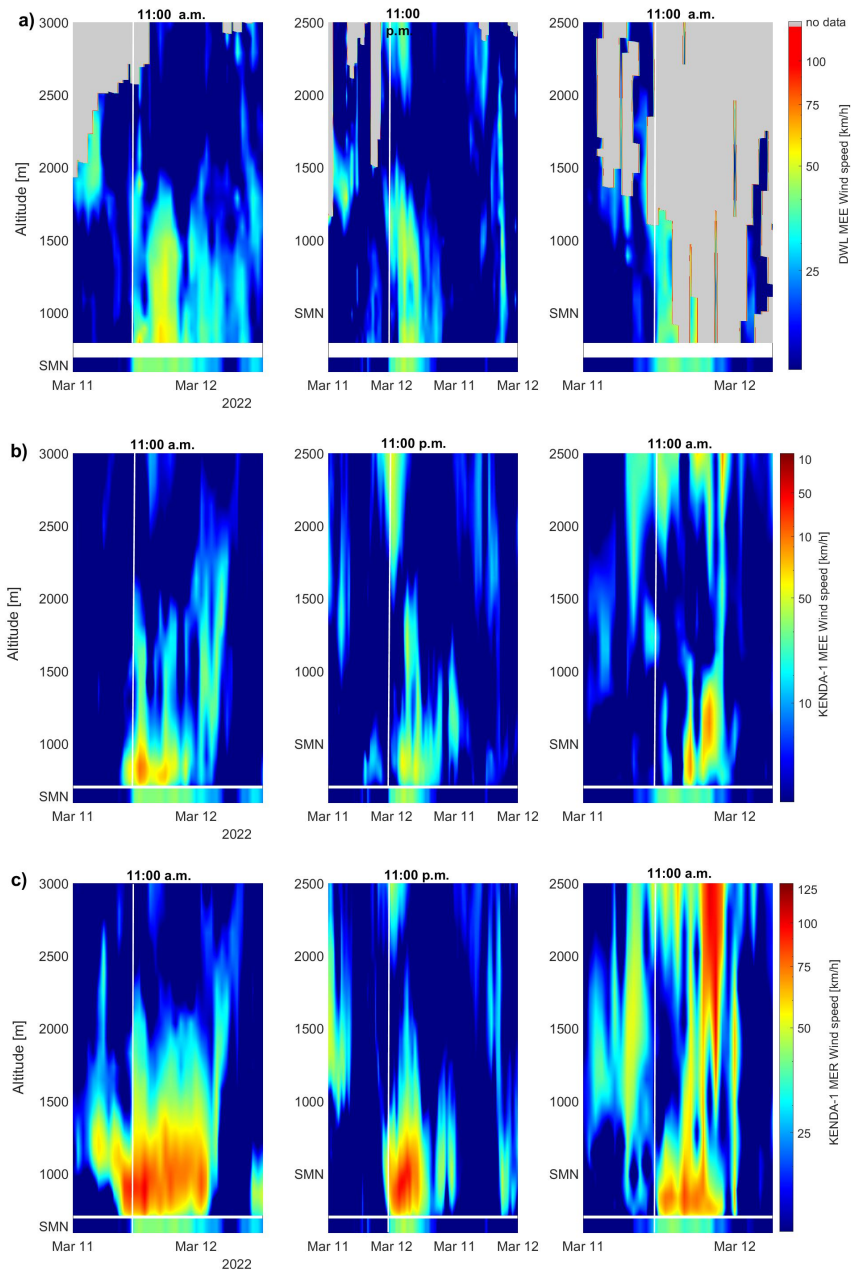
Figure 12. Wind speed profiles [km/h] time series from a) DWL/MEE, b) KENDA-1/MEE and c) KENDA-1/MER during a selection of 3 foehn events: left 11-12.03.2022, middle 19-22.03.2022 and right 23-24.04.2022. Wind speeds [km/h] from the SMN/MER are given in the lower part of each figure. The solid line represents the foehn breakthrough.

4 Discussion

Complex topography, landscape heterogeneity and specific thermal wind regimes challenge the models' spatial and temporal resolutions, their performance in data assimilation and the parameterization of multi-scale processes. The discussion will consequently focus on three points, the specificity of the terrain around the campaign site, the comparison of the observed wind and T profiles with previous observations in the Alps and the model performances in Meiringen.

4.1 Topographical and methodological challenges

The Haslital presents several peculiar topographical and landscape characteristics, particularly in the vicinity of the campaign site (Fig. 1). Its junction with the Sarneraatal via the Brünig Pass links the two valleys with an angle of $\sim 90°$, 400 m above the valley floor. It allows winds from the Sarneraatal to easily reach the Haslital with a cross-valley wind component similar to down slope winds and to disturb its along valley wind system. The location of MEE just under the Brünig Pass has to be taken into account for comparison between MEE and MER results. Based on numerical simulation in the Alpine Inn Valley, Zängl (2004) suggests that variations in wind intensity are mainly related to tributary valleys, which increase or decrease the mass flux in the main valley. In this regard, low passes can have similar effects as tributaries. Moreover, the model cell over MEE overlaps the slope towards the Brünig Pass, so that KENDA-1/MEE reports an overlay of winds from the Brünig Pass and in the Haslital. DWL/MEE, on the other hand, only observes winds in the middle of the Haslital. Consequently, the differences between the modeled T/wind averaged values and the observations cannot be only considered as model errors only.

Additionally, the curving of the valley between MER and MEE implies that the same valley side faces different orientations along the Haslital leading to different heating by the incoming solar radiation. The presence of large lakes covering the entire valley floor in its lower part, 5 km down valley of MEE, modifies the heat exchange between the surface and the atmosphere due to their high thermal inertia. Their influence on the T along the valley can affect the pressure difference, and consequently the time, extent and strength of the thermally induced valley winds. When comparing observed phenomena with similar studies, the combination of the above mentioned peculiar features gives explanatory hints for the observed differences. Finally, this study is based on monthly median values, so that the averaging artifacts have to be considered, e.g. for the analysis of maximum wind speed, the onset time of valley wind or wind directions. In that sense, this analysis focused on climatology and not on the forecast skills of COSMO-1E.

4.2 Comparison of observed phenomena with other studies

4.2.1 Occurrence of surface based T inversion in valleys

T patterns in MER follow a classical diurnal and seasonal cycle. The most important feature in the context of this study is the presence of frequent ground T inversion (Fig. 2.a, 5.a). According to a 3 years study in the French Jura performed over 16 station pairs at different altitudes (Joly and Richard, 2019), T-inversions are equally common in winter and summer (60% of the time), but with a larger amplitude (3°C) in winter than in summer (2°C). Additionally, temperature inversion occurred also more

than 50% of the time in a 13 years T climatology in the Cascade Range, USA, at comparable altitudes (Rupp et al., 2020), with the formation and dissipation of inversions consistently having an approximately four hours time difference from sunset and sunrise. Finally, a 56-year climatology in the Austrian Alps (Hiebl and Schöner, 2018), shows that T inversions occur throughout the year with a frequency of about 30% from October to January and 15% from April to August. The intensity, magnitude and thickness of these surface T inversions follow a similar seasonal pattern as observed in the Haslital. Inversions are more frequent in eastern Austria and less frequent in the wide western valleys and basins and almost vanishing in high-Alpine summit area. This campaign (Nov-Aug) in the Haslital (Fig. 5.a) shows a similar occurrence of near ground T inversions, i.e. 30% between the two ground stations (MER-BRU) and 40% in the MWR profiles. Amplitudes are similar to the results from Joly and Richard (2019) with slightly higher values during winter months (+ 1°C). The seasonality of the phenomena is mainly characterized by the frequency of T inversions along the day in winter and the onset of the erosion process. Similar seasonality as in Austria (Hiebl and Schöner, 2018) are found with 14.3% of T inversions from April to August and 46% from November to February.

4.2.2 Characteristics of valley winds in the Alps

Previous studies on diurnal valley winds in alpine valleys took place in the Rhone (Length = 140 km, Floor Width = 4-5 km, Ridge to Ridge Width = 15 km, Schmid et al. (2020)), in the Adige (L = 140 km, BW = 2-3 km, RRW = 8 km, Giovannini et al. (2017)) and in the Inn valleys (L = 140 km, BW = 4-5 km, RRW = 20 km, Adler et al. (2021)). These three valleys are relatively long and wide compared to the Haslital (L = 30 km, BW = 1.5 km, RRW = 5 km), which can induce differences in the thermal valley wind systems. All three studies make a selection of valley wind days by using threshold on minimum global solar radiation or up valley wind speeds and selected global weather type.

Similarly to the observations in the Haslital, the wind direction change in the Rhone valley (Schmid et al., 2020) occurs for altitudes up to about 2 km a.g.l. with diurnal pattern undergoing significant changes during the course of the year. During summer, maximum up valley speeds of 30-35 km/h are found above the Rhone valley during the early afternoon at 200 m a.g.l. Similar timing for maximum up valley winds are found at both MER and MEE, but with reduced speeds both at ground (SMN/MER, 20-30 km/h) and at 200-300 m a.g.l. (DWL/MEE, 15-20 km/h) that relates to some extend to the absence of clear-sky days selection in this study. At MEE, the highest wind speeds of 30 to 45 km/h are found however later on, at 18:00 and 19:00, between 800 and 1400 m and correspond to valley winds from the Sarneraatal. The topographic difference between the Brünig Pass and the standard tributaries' inlet at the campaign site in Sion can also explain the time and altitude differences of the strongest winds. Concerning down valley wind speeds, Schmid et al. (2020) report their presence between 500 and 1000 m.a.g.l with a speed of about 15-20 km/h. They occur in the second part of the night in spring and summer, and during the entire night in winter. Several differences are observed in the Haslital: 1) down valley winds reach ground even in summer (Fig. 7) and extend up to 800-1000 m.a.g.l., 2) their speed gradually decrease around the night with almost no wind between 00:00 and the new onset of up valley winds for all the studied period and 3) at MEE, maximum down valley wind speeds are measured from March to July at the same altitude as in the Rhone valley but with lower wind speeds (10-15 km/h). If the last difference can also be explained by the applied monthly average, the timing and extent of the down valley winds probably relates to topography differences.

In the Adige valley in the Italian Alps, a campaign in May-August (Giovannini et al., 2017) observed maximum up valley wind speeds between 15:00 and 16:00 that are stronger near the valley outlet (20-30 km/h) and gradually weaken (8-10 km/h) towards the highest valley parts situated 100 km further up. Surface down valley wind speed appears to be very weak, between 0 and 5 km/h, and nearly constant in the entire valley. However, contrarily to the Haslital and the Rhone valley, the down valley wind onset is delayed to 00:00. Wind profiler data from the outlet of the Adige valley show that the strongest up valley winds are recorded in the late afternoon, similarly to the observations at MEE (Fig.8.a). Contrarily to both, Schmid et al. (2020) and this study, the down valley winds of the Adige valley gradually weaken towards higher altitudes around midnight. For the rest of the night, stronger wind are also found between 500 and 1000 m.a.g.l. similarly to the observation in the Rhone valley (Schmid et al., 2020).

Finally, concerning the onset of up valley wind, both the time and the pattern of the transition are similar in the Rhone, the Adige and the Haslital valley. The onset occurs 3-4 hours after sunrise with flows that move almost simultaneously between 0 to 1500 m.a.g.l from June onwards. The morning transition occurs at the same time at all heights while, during the evening transition, down wind begins at ground due to progressive cooling of the lowest atmospheric layer (Zängl, 2004) and thickens during the night. Note that, Schmid et al. (2020) reported a delayed onset as a function of altitude in autumn but unfortunately, no data were acquired during this period in the Haslital.

The CROSSINN campaign (Adler et al., 2021) was performed from August to October in the lower part of the Inn valley and focused on cross valley winds. During two days of September, the wind field in the vertical plane across the valley show subsidence around 13:30 and 14:30 without any particular cross valley wind direction above the valley floor center. In the second part of the afternoon (15:00-17:00), the valley atmosphere presents an enhanced cross valley wind circulation. Over the south facing slope of the valley, subsidence prevails, while over the north facing slope upward motion is measured. This flow pattern form a closed circulation cell with a clear cross-valley component comprising a northerly component in the lower 700 m.a.g.l. and a southerly component above. Similarly to the Inn valley, the Haslital at MEE also lies in the E-W direction. A cross-valley circulation is also observed from March to August (Fig. 9.a), with a wind direction change from N to S between 450 and 850 m a.g.l and a stronger pattern in Summer. However, in MEE, valley winds from the Sarneraatal are probably the main drivers of this circulation cell at sunset.

4.3   Model performance

According to the presented monthly median values, KENDA-1 is generally able to capture the main features of the observed atmospheric conditions and the differences to the observations are comparable to those found in standard MeteoSwiss seasonal verification with radiosonde and surface observations averaged over the whole model domain. This is remarkable given the complex topography in the region of this study. However, some meteorological phenomena specific to mountainous regions and/or particular synoptic conditions are hard to capture by the model and thus can lead to larger differences between model and observations.

4.3.1 KENDA-1 skills in temperature estimate

The analysis of the daily cycle shows that the majority of ground T differences with respect to observations lays between ± -3 °C (Fig. 4) with a nighttime overestimation and a daytime underestimation by KENDA-1. In a study over complex topography (Alpine Arc and particularly Switzerland and northern Italy) Voudouri et al. (2021) found a similar daily cycle in ground T mean error in COSMO-1E forecasts, but of reduced amplitude (-0.5 °C bias during day and a +0.5 °C bias during night). Despite the complex topography around MER and the induced elevation bias, the modeled climatology of ground T is comparable to standard verification results, even if differences up to 8° C are found in some periods. The main explained source of ground T differences is caused by missed surface T inversion. The frequency of this phenomenon is partially missed by KENDA-1 from March to August (Fig. 5.a) and its amplitude is underestimated for all months. This is especially the case at the end of March, when enhanced night time radiative cooling and important global solar radiation form strong inversions. The observed amplitude difference are mainly due to an underestimation of T at ground (Fig. 4). A work carried by Sekula et al. (2019) on the nonhydrostatic model CY40T1 AROME CMC (2km horizontal resolution) showed the same general overestimation of the minimum T in valleys bottom. The largest differences were measured during strong high-pressure systems which favors cold air pools formation leading to T overestimations of up + 7 to 9°C during 10 days in March.

A preliminary analysis on KENDA-1 behaviour during this strong T inversions show that the observed differences are probably due to a too low model first guess ensemble spread. The model is too much trusted in the model-observation weighting scheme and measured T at MER are therefore not used in the model assimilation step. Another hypothesis is that a too large observation error is assigned to the station of MER (1.17K end of March). Additionally, at this period, the difference between observed and modeled ground relative humidity (RH) are within $\pm$ 5% during day but, during night, the model is heavily drier (-20 to -30 % RH, not shown). According to Westerhuis et al. (2021), artifacts from the NWP can be expected under conditions favourable to surface T-inversion. The COSMO-1E vertical coordinates follow the terrain. Therefore, in complex topography, numerical artifacts may originate from the intersection between T-inversions and the surface of the vertical grid used by the model. The systematic T underestimation during night can also be driven by an overestimated modeled cloudiness involving underestimated out-going long-wave radiation. Further investigations have to be performed using ceilometer and/or DWL observations to estimate the model skill with respect to cloud cover. Finally, the differences with observations can also originate from a modeled ongoing turbulent mixing whereas in reality a cold pool with a full or partial decoupling from the above flow is present in the valley.

For profile comparison, MWR T is taken as the reference, but its reliability, especially at high altitude, has to be considered in the evaluation of KENDA-1 results. Löhnert and Maier (2012) performed a MWR-RS comparison and showed that random error inherent to the measurement principle can be important in some cases. They showed that random errors range grows up to 1.7 K at 4 km height, due to a 95% influence from the used apriori profile. KENDA-1 and MWR T profiles differences are constrained to $\pm$ 1 °C for all altitudes between 1400 and 2200 m both day and night except in June and July (Fig. 2.b). Differences up to -3 °C can occur near the ground in winter or at ridge level in July. The near overall negative bias can mainly be explained by two factors: first, the MWR is susceptible of errors especially for higher altitudes with RMSE between 1 and 1.5 °C (Liu et al.,

625 2022) and, second, the MWR/MEE has been trained with profiles from Payerne, so that the difference in altitude between both stations (+100 m) and in atmospheric conditions could induce a larger RMSE or even a bias in the MWR measurements. Despite these uncertainties, the T differences up to -3 °C are probably a clear underestimation of KENDA-1 Ts. The hypothesis of cloud amount overestimation mentioned before can also explain this T profile bias.

4.3.2   KENDA-1 skill in wind estimate

630 The monthly valley wind reveals a good performance of the model. Up and down-valley wind are in good agreement with the observations from March to July and, to a lesser extent, in November. KENDA-1 is also able to get the seasonal evolution of the vertical extent of the valley wind system. The onset of up valley winds is however predicted too early after sunrise (Fig. 6 and 8). This 1-2 hours difference with the observations is partially explained by the absence of surface T inversion in the model (sect. 3.1.3), so the time allowing an erosion of the stable layer is not taken into account.

635 The capability of COSMO models to estimate the diurnal along-valley winds in real valleys has been investigated by Schmidli et al. (2018) for 3 summer weeks with weak synoptic forcing and intense solar heating. The model results are compared to observations at the MeteoSwiss ANETZ stations, the automatic monitoring network preceding the present-day SMN. They showed that the wind diurnal cycle is well represented by COSMO1-E in large valleys such as the Rhine Valley at Chur (base width of 3 km and width at half height of 8 km), and medium valleys (e.g. the Rhone Valley at Visp a with base width of 1 km

640 and width at half height of 4 km). For smaller valleys, e.g. the Maggia Valley in Cevio (base width of 500 m, width at half-height of 3 km), the valley wind amplitude was underestimated. Despite an underestimation of the maximal valley wind speed, the onset of up and down valley winds was correctly modeled. The results of the modeled wind speed and direction at MEE are comparable to the analysis in Visp (Fig. 8), a valley with a similar cross-section. However, the onset of up and down valley winds is in less agreement with the observations at Meiringen, probably due to the four time shorter length of the Haslital and its

645 topographic peculiarities.

The differences between KENDA-1 and the observed cross-valley wind climatology (Fig. 9) can be interpreted as a too strong modeled influence of the Sarneraatal thermal winds or as an effect of the grid cell overlap on the north-facing slope. The presence of strong down slope winds at the Brünig Pass may have a direct influence on the along valley wind diurnal cycle. In a recent study in the Rhone valley at Sion, Schmidli and Quimbayo-Duarte (2023) reports a correctly modeled evening

650 transition but an inadequate representation of the morning wind reversal by COSMO-1E. Like in the Haslital (Fig. 9), too strong modeled cross-valley wind reaching the valley floor interrupt the formation of the up-valley flows for certain days. At Sion, the cross-valley flow is restricted to upper levels so that the stronger lower valley atmosphere stratification protects the up-valley flow.

According to (Schmidli et al., 2018), the horizontal resolution required for a good along valley wind representation requests

655 at least 1-2 grid cells in the valley base cross section. A more important feature is the altitude bias of the model at the ground. For the MER station, the width of the valley can contain 1.5 grid cells (Fig. 1) but the fact that no cell contains only the valley floor leads to this disfavouring bias in altitude. Surface atmospheric moisture is a key factor of stratification, which in turn favors the cross valley winds influence. Simulations performed by Schmidli and Quimbayo-Duarte (2023) show that a 30% increased

soil moisture relative to KENDA-1 data leads to better along valley wind modeling. Even though stronger smoothing of the topography improves the stratus cloud simulations, it also decrease the quality of forecasts of valley winds and orographically induced convection (Westerhuis et al., 2021).

Finally, despite the fact that KENDA-1 proposes good monthly median values, the case-by-case analysis shows important differences with observations. Non-systematic differences are observed in most profiles. Even thought these differences show regular patterns in the case of foehn or valley winds, it is common that unpredictable behavior affects the model.

5   Conclusion

The extensive measurement campaign in MER yields valuable information on the diurnal and seasonal cycles of wind and T profiles that were not available in this region and that are rather sparse in alpine middle size valleys. The observations of the MWR, DWL and of the nearby SMN stations allowed to determine the particularities of the Haslital valley between November 2021 and July 2022. In parallel to these observations, the data of two cells of the KENDA-1 assimilation model has been analyzed and compared to the measurements.

Regarding the observed and modeled T, the main results concerns the surface based T inversion. Nighttime T inversions are commonly observed during all the months under study with bigger amplitudes during December and January and a persistence during daytime from November to February. The frequency of occurrence and the amplitude of the surface T inversions are both underestimated in the T profiles of KENDA-1. This results in a systematic overestimation of the ground T during the presence of surface based inversions. In extreme cases it reaches up to 8 °C. This large model error has an important consequence, since the discrepancies between the model first guess prevents the SMN/MER observations to be assimilated. The differences between MWR/MEE and KENDA-1/MEE profiles are small with a T underestimation of -2 to -3 °C under 1500 m that is more frequent during nighttime.

Regarding the wind, thermal valley winds are observed in the monthly wind direction for all the months under study except in December and January. This diurnal flow patterns develop in a more distinct way for the summer months (June to August). The vertical extent of down-valley winds after sunset increases from March to August: from 1000 m a.g.l. to 1600 m a.g.l. respectively. The morning transition to up valley wind is delayed by about 3-4 hours compared to sunrise and is near simultaneous for the rest of the profile. The onset of down valley winds happens less than an hour before sunset and propagates from ground to ridge height in some hours. In addition, this thermal wind system can be influenced by external factors such as synoptic wind intrusions or perturbation from adjacent valleys wind system. At MEE, N winds from the tributary valley (Sarneraatal) through the low altitude Brünig Pass are observed from mid-afternoon to sunset. At MEE, they affect the evening transition and sometimes even the along valley wind pattern during daytime below the altitude of the pass. If these N flows only slightly modify the up valley wind direction at MER, they are able to suppress the up valley winds at BRZ. In summer, a cross valley circulation is measured around sunset (19:00-20:00) at MEE with a separation between north and south facing wind between 700 and 1000 m a.g.l. The formation of this closed circulation cell is influenced by the strong wind from the Sarneraatal.

The comparison with observations shows that KENDA-1 was able to simulate median directions and speeds of the diurnal valley winds. The vertical extent of the thermal winds, the onset time of down valley winds and the interaction with synoptic winds are also appropriately modeled. However, KENDA-1 shows a too early (1-2 hours) onset of up-valley winds due to the absence of the near surface stable layer caused by the nighttime inversion. Moreover, the observed cross circulation in MEE at sunset is not modeled by KENDA-1.

Contrarily to monthly values, the analysis of single profiles shows important differences between the model and the measurements. This is particularly true during foehn events with a near systematic underestimation of 2 to 4°C by KENDA-1 in both the ground and the profile temperatures. Wind speeds simulation during foehn show significant difference over MEE and MER: the KENDA-1/MEE show a good match up to 1000 m a.g.l. whereas KENDA-1/ MER reports wind speed twice higher (120 km/h). A detailed analysis of three clear sky summer days also allows to underline clear differences between the observations and the model concerning the wind direction (up to 90°), the wind speed (up to 30 km/h) and the timing (up to 4-6 h) of the along valley transition.

The results obtained in this study allowed to deepen consensual knowledge about atmospheric phenomena in complex topography and to identify processes specific to the studied valley. Complex interactions between the Haslital and the tributary valley of the Sarneraatal have been observed and could explain some differences observed with the literature. However, many observed phenomena are not yet satisfactorily characterized and modeled and require further investigation. A better understanding of the exchange processes in complex topography and the ability of the model to take them into account is an essential condition to improve the prediction capacity of NWP in mountainous terrain.

Data availability.   Data are available on request

Author contributions.   AB did the analysis, AB and MCC prepared the manuscript. MH and SM operated the instruments during the campaign. DL and MA provided the model data. All co-authors contributed to the manuscript online.

Competing interests.   The authors declare that they have no conflict of interest.

Acknowledgement.   This work was supported by the the Swiss Federal Office for Meteorology and Climatology

References

Adler, B., Gohm, A., Kalthoff, N., Babić, N., Corsmeier, U., Lehner, M., Rotach, M. W., Haid, M., Markmann, P., Gast, E., Tsaknakis, G., and Georgoussis, G.: CROSSINN: A Field Experiment to Study the Three-Dimensional Flow Structure in the Inn Valley, Austria, Bull. Amer. Meteor. Soc., 102, E38 – E60, https://doi.org/10.1175/BAMS-D-19-0283.1, 2021.

Baldauf, M., Seifert, A., Förstner, J., Majewski, D., Raschendorfer, M., and Reinhardt, T.: Operational Convective-Scale Numerical Weather Prediction with the COSMO Model: Description and Sensitivities, Monthly Weather Review, 139, 3887 – 3905, https://doi.org/https://doi.org/10.1175/MWR-D-10-05013.1, 2011.

Chachere, C. N. and Pu, Z.: Connections Between Cold Air Pools and Mountain Valley Fog Events in Salt Lake City, Pure Appl. Geophys., 173, 3187–3196, https://doi.org/10.1007/s00024-016-1316-x, 2017.

Chow, F. K., Weigel, A. P., Street, R. L., Rotach, M. W., and Xue, M.: High-Resolution Large-Eddy Simulations of Flow in a Steep Alpine Valley. Part I: Methodology, Verification, and Sensitivity Experiments, J. Appl. Meteor. Climatol., 45, 63 – 86, https://doi.org/10.1175/JAM2322.1, 2006.

Colette, A., Chow, F. K., and Street, R. L.: A Numerical Study of Inversion-Layer Breakup and the Effects of Topographic Shading in Idealized Valleys, J. Appl. Meteor., 42, 1255 – 1272, https://doi.org/https://doi.org/10.1175/1520-0450(2003)042<1255:ANSOIB>2.0.CO;2, 2003.

Crezee, B., Merker, C., Daniel, R., Leuenberger, D., Vural, J., Haefele, A., Hervo, M., Martucci, G., Bättig, P., and Arpagaus, M.: Assimilation of ground-based remote sensing profiler data at MeteoSwiss, EMS Annual Meeting Abstracts, 19, https://doi.org/10.5194/ems2022-568, 2022.

De Wekker, S. F. J. and Kossmann, M.: Convective Boundary Layer Heights Over Mountainous Terrain—A Review of Concepts, Frontiers in Earth Science, 3, https://doi.org/10.3389/feart.2015.00077, 2015.

Diémoz, H., Barnaba, F., Magri, T., Pession, G., Dionisi, D., Pittavino, S., Tombolato, I. K. F., Campanelli, M., Della Ceca, L. S., Hervo, M., Di Liberto, L., Ferrero, L., and Gobbi, G. P.: Transport of Po Valley aerosol pollution to the northwestern Alps – Part 1: Phenomenology, Atmos. Chem. Phys., 19, 3065–3095, https://doi.org/10.5194/acp-19-3065-2019, 2019.

Duine, G.-J., Hedde, T., Roubin, P., Durand, P., Lothon, M., Lohou, F., Augustin, P., and Fourmentin, M.: Characterization of valley flows within two confluent valleys under stable conditions: observations from the KASCADE field experiment, Quart. J. Roy. Meteor. Soc., 143, 1886–1902, https://doi.org/10.1002/qj.3049, 2017.

Dürr, B.: Automatisiertes Verfahren zur Bestimmung von Föhn in Alpentälern, Tech. rep., Arbeitsberichte der MeteoSchweiz, https://www.meteoschweiz.admin.ch/dam/jcr:3ed2aec8-0901-417a-acc3-8be11cce440a/Foehnindex_Arbeitsbericht_223_Automatisiertes_Verfahren_zur_Bestimmung_von_Foehn_in_Alpentaelern_de.pdf, 2008.

Giovannini, L., Laiti, L., Serafin, S., and Zardi, D.: The thermally driven diurnal wind system of the Adige Valley in the Italian Alps, Quart. J. Roy. Meteor. Soc., 143, 2389–2402, https://doi.org/10.1002/qj.3092, 2017.

Hauge, G.: High resolution weather forecasting and predictability - applications in complex terrain, Ph.D. thesis, University of Bergen, Sweden, https://core.ac.uk/download/pdf/30925119.pdf, 2006.

Hervo, M., Bättig, P., and Haefele, A.: Evaluation of the new microwave radiometer HATPRO-G5., Tech. rep., Federal Office of Meteorology and Climatology, MeteoSwiss, Payerne, Switzerland, 2021.

Hiebl, J. and Schöner, W.: Temperature inversions in Austria in a warming climate changes in space and time, Meteorologische Zeitschrift, 27, https://doi.org/10.1127/metz/2018/0899, 2018.

Hunt, B. R., Kostelich, E. J., and Szunyogh, I.: Efficient data assimilation for spatiotemporal chaos: A local ensemble transform Kalman filter, Physica D: Nonlinear Phenomena, 230, 112–126, https://doi.org/10.1016/j.physd.2006.11.008, 2007.

Jacques-Coper, M., Falvey, M., and Muñoz, R. C.: Inter-daily variability of a strong thermally-driven wind system over the Atacama Desert of South America: synoptic forcing and short-term predictability using the GFS global model, Theor. and Appl. Clim., 121, 211–223, https://doi.org/10.1007/s00704-014-1231-y, 2015.

Jansing, L., Papritz, L., Dürr, B., Gerstgrasser, D., and Sprenger, M.: Classification of Alpine south foehn based on 5 years of kilometre-scale analysis data, Weather and Climate Dyn., 3, 1113–1138, https://doi.org/10.5194/wcd-3-1113-2022, 2022.

Joly, D. and Richard, Y.: Topographic descriptors and thermal inversions amid the plateaus and mountains of the Jura (France), Climatologie, 15, 46–61, https://doi.org/10.4267/climatologie.1335, 2018.

Joly, D. and Richard, Y.: Frequency, intensity, and duration of thermal inversions in the Jura Mountains of France, Theor. Appl. Climatol., 138, 639–655, https://doi.org/10.1007/s00704-019-02855-3, 2019.

Kossmann, M. and Sturman, A.: Pressure-Driven Channeling Effects in Bent Valleys, J. Appl. Meteorol., 42, 151–158, https://doi.org/10.1175/1520-0450(2003)042<0151:PDCEIB>2.0.CO;2, 2003.

Krishnamurthy, R., Calhoun, R., Billings, B., and Doyle, J.: Wind turbulence estimates in a valley by coherent Doppler lidar, Meteor. Appl., 18, 361–371, https://doi.org/10.1002/met.263, 2011.

Lang, M. N., Gohm, A., and Wagner, J. S.: The impact of embedded valleys on daytime pollution transport over a mountain range, Atmos. Chem. Phys., 15, 11 981–11 998, https://doi.org/10.5194/acp-15-11981-2015, 2015.

Langhans, W., Schmidli, J., Fuhrer, O., Bieri, S., and Schär, C.: Long-Term Simulations of Thermally Driven Flows and Orographic Convection at Convection-Parameterizing and Cloud-Resolving Resolutions, J. Appl. Meteor. Climatol., 52, 1490 – 1510, https://doi.org/10.1175/JAMC-D-12-0167.1, 2013.

Lehner, M. and Rotach, M. W.: Current Challenges in Understanding and Predicting Transport and Exchange in the Atmosphere over Mountainous Terrain, Atmosphere, 9, https://doi.org/10.3390/atmos9070276, 2018.

Leuenberger, D., Koller, M., Fuhrer, O., and Schär, C.: A Generalization of the SLEVE Vertical Coordinate, Mon. Wea. Rev., 138, 3683 – 3689, https://doi.org/10.1175/2010MWR3307.1, 2010.

Liu, M., Liu, Y.-A., and Shu, J.: Characteristics Analysis of the Multi-Channel Ground-Based Microwave Radiometer Observations during Various Weather Conditions, Atmosphere, 13, https://doi.org/10.3390/atmos13101556, 2022.

Lute, A. C. and Abatzoglou, J. T.: Best practices for estimating near-surface air temperature lapse rates, Int. J. Climatol., 41, E110–E125, https://doi.org/10.1002/joc.6668, 2021.

Löhnert, U. and Maier, O.: Operational profiling of temperature using ground-based microwave radiometry at Payerne: prospects and challenges, Atmos. Meas. Tech., 5, 1121–1134, https://doi.org/10.5194/amt-5-1121-2012, 2012.

Löhnert, U., Knist, C., Böck, T., and Pospichal, B.: Microwave Radiometer Observations during FESSTVaL 2021, https://doi.org/10.25592/uhhfdm.10198, Project: FESSTVaL (Field Experiment on submesoscale spatio-temporal variability in Lindenberg), a measurement campaign initiated by the Hans-Ertel-Center for Weather Research., 2022.

Martinet, P., Cimini, D., De Angelis, F., Canut, G., Unger, V., Guillot, R., Tzanos, D., and Paci, A.: Combining ground-based microwave radiometer and the AROME convective scale model through 1DVAR retrievals in complex terrain: an Alpine valley case study, Atmos.Meas. Tech., 10, 3385–3402, https://doi.org/10.5194/amt-10-3385-2017, 2017.

Miró, J. R., Peña, J. C., Pepin, N., Sairouni, A., and Aran, M.: Key features of cold-air pool episodes in the northeast of the Iberian Peninsula (Cerdanya, eastern Pyrenees), Int. J. of Climatol., 38, 1105–1115, https://doi.org/https://doi.org/10.1002/joc.5236, 2018.

Rose, T., Crewell, S., Löhnert, U., and Simmer, C.: A network suitable microwave radiometer for operational monitoring of the cloudy atmosphere, Atmos. Res., 75, 183–200, https://doi.org/10.1016/j.atmosres.2004.12.005, 2005.

790 Rotach, M. W., Gohm, A., Lang, M. N., Leukauf, D., Stiperski, I., and Wagner, J. S.: On the Vertical Exchange of Heat, Mass, and Momentum Over Complex, Mountainous Terrain, Frontiers in Earth Science, 3, https://doi.org/10.3389/feart.2015.00076, 2015.

Rotach, M. W., Serafin, S., Ward, H. C., Arpagaus, M., Colfescu, I., Cuxart, J., De Wekker, S. F. J., Grubišić, V., Kalthoff, N., Karl, T., Kirshbaum, D. J., Lehner, M., Mobbs, S., Paci, A., Palazzi, E., Bailey, A., Schmidli, J., Wittmann, C., Wohlfahrt, G., and Zardi, D.: A Collaborative Effort to Better Understand, Measure, and Model Atmospheric Exchange Processes over Mountains, Bulletin of the American

795 Meteorological Society, 103, E1282 – E1295, https://doi.org/https://doi.org/10.1175/BAMS-D-21-0232.1, 2022.

Rupp, D. E., Shafer, S. L., Daly, C., Jones, J. A., and Frey, S. J. K.: Temperature Gradients and Inversions in a Forested Cascade Range Basin: Synoptic- to Local-Scale Controls, J. Geophys. Res. Atmos., 125, e2020JD032 686, https://doi.org/10.1029/2020JD032686, 2020.

Saigger, M. and Gohm, A.: Is it north or west foehn? A Lagrangian analysis of Penetration and Interruption of Alpine Foehn intensive observation period 1 (PIANO IOP 1), Weather and Climate Dyn., 3, 279–303, https://doi.org/10.5194/wcd-3-279-2022, 2022.

800 Schmid, F., Schmidli, J., Hervo, M., and Haefele, A.: Diurnal Valley Winds in a Deep Alpine Valley: Observations, Atmosphere, 11, https://doi.org/10.3390/atmos11010054, 2020.

Schmidli, J. and Quimbayo-Duarte, J.: Diurnal Valley Winds in a Deep Alpine Valley: Model Results, Meteorology, 2, 87–106, https://doi.org/10.3390/meteorology2010007, 2023.

Schmidli, J. and Rotunno, R.: Mechanisms of Along-Valley Winds and Heat Exchange over Mountainous Terrain, J. Atmos. Sci., 67, 3033 –

805 3047, https://doi.org/10.1175/2010JAS3473.1, 2010.

Schmidli, J., Böing, S., and Fuhrer, O.: Accuracy of Simulated Diurnal Valley Winds in the Swiss Alps: Influence of Grid Resolution, Topography Filtering, and Land Surface Datasets, Atmosphere, 9, https://doi.org/10.3390/atmos9050196, 2018.

Schnitzhofer, R., Norman, M., Wisthaler, A., Vergeiner, J., Harnisch, F., Gohm, A., Obleitner, F., Fix, A., Neininger, B., and Hansel, A.: A multimethodological approach to study the spatial distribution of air pollution in an Alpine valley during wintertime, Atmos. Chem. Phys.,

810 9, 3385–3396, https://doi.org/10.5194/acp-9-3385-2009, 2009.

Schraff, C., Reich, H., Rhodin, A., Schomburg, A., Stephan, K., Periáñez, A., and Potthast, R.: Kilometre-scale ensemble data assimilation for the COSMO model (KENDA), Quart. J. Roy. Meteor. Soc., 142, 1453–1472, https://doi.org/10.1002/qj.2748, 2016.

Sekula, P., Bokwa, A., Bochenek, B., and Zimnoch, M.: Prediction of Air Temperature in the Polish Western Carpathian Mountains with the ALADIN-HIRLAM Numerical Weather Prediction System, Atmosphere, 10, https://doi.org/10.3390/atmos10040186, 2019.

815 Serafin, S., Adler, B., Cuxart, J., De Wekker, S. F. J., Gohm, A., Grisogono, B., Kalthoff, N., Kirshbaum, D. J., Rotach, M. W., Schmidli, J., Stiperski, I., Večenaj, , and Zardi, D.: Exchange Processes in the Atmospheric Boundary Layer Over Mountainous Terrain, Atmosphere, 9, https://doi.org/10.3390/atmos9030102, 2018.

Sfyri, E., Rotach, M. W., Stiperski, I., Bosveld, F. C., Lehner, M., and Obleitner, F.: Scalar-Flux Similarity in the Layer Near the Surface Over Mountainous Terrain, Boundary-Layer Meteorology, 169, 11–46, https://doi.org/10.1007/s10546-018-0365-3, 2018.

820 Stephan, K., Klink, S., and Schraff, C.: Assimilation of radar-derived rain rates into the convective-scale model COSMO-DE at DWD, Quart. J. Roy. Meteor. Soc., 134, 1315–1326, https://doi.org/10.1002/qj.269, 2008.

Tian, Y., Schmidli, J., and Quimbayo-Duarte, J.: A station-based evaluation of south foehn forecasting with COSMO-1, EGU General Assembly, Vienna, Austria, https://doi.org/10.5194/egusphere-egu22-3680, 2022.

Vosper, S., Carter, E., Lean, H., Lock, A., Clark, P., and Webster, S.: High resolution modelling of valley cold pools, Atmos. Sci. Letters, 14,

825 193–199, https://doi.org/https://doi.org/10.1002/asl2.439, 2013.

Voudouri, A., Avgoustoglou, E., Carmona, I., Levi, Y., Bucchignani, E., Kaufmann, P., and Bettems, J.-M.: Objective Calibration of Numerical Weather Prediction Model: Application on Fine Resolution COSMO Model over Switzerland, Atmosphere, 12, https://doi.org/10.3390/atmos12101358, 2021.

Wagner, J. S., Gohm, A., and Rotach, M. W.: The Impact of Horizontal Model Grid Resolution on the Boundary Layer Structure over an Idealized Valley, Mon. Wea. Rev., 142, 3446 – 3465, https://doi.org/10.1175/MWR-D-14-00002.1, 2014.

Wang, Y., Hocut, C. M., Hoch, S. W., Creegan, E., Fernando, H. J. S., Whiteman, C. D., Felton, M., and Huynh, G.: Triple Doppler wind lidar observations during the mountain terrain atmospheric modeling and observations field campaign., J. Appl. Rem. Sens., 10, https://doi.org/10.1117/1.JRS.10.026015, 2016.

Westerhuis, S., Fuhrer, O., Bhattacharya, R., Schmidli, J., and Bretherton, C.: Effects of terrain-following vertical coordinates on simulation of stratus clouds in numerical weather prediction models, Quart. J. Roy. Meteor. Soc., 147, 94–105, https://doi.org/10.1002/qj.3907, 2021.

Whiteman, C. D.: Observations of Thermally Developed Wind Systems in Mountainous Terrain, Environmental Science, pp. 5–42, https://doi.org/10.1007/978-1-935704-25-6_2, 1990.

Zardi, D. and Whiteman, C. D.: Observations of thermally developed wind systems in mountainous terrain. Mountain Weather Research and Forecasting—Recent Progress and Current Challenges, Springer: Berlin, Germany, pp. 35–122, 2013.

Zängl, G.: A reexamination of the valley wind system in the Alpine Inn Valley with numerical simulations, Meteor. Atmos. Phys., 87, 241–256, https://doi.org/10.1007/s00703-003-0056-5, 2004.